

Review

# Electrolytes for Aqueous Zn-Ion Batteries Working in Wide-Temperature Range: Progress and Perspective

Lixia Sun <sup>1</sup>, Zhongcheng Song <sup>1</sup>, Chao Deng <sup>1</sup>, Qiang Wang <sup>1</sup>, Funian Mo <sup>2,\*</sup>, Haibo Hu <sup>3,\*</sup> and Guojin Liang <sup>4,\*</sup><sup>1</sup> School of Chemistry and Chemical Engineering, Jiangsu University of Technology, Changzhou 213001, China<sup>2</sup> Shenzhen Key Laboratory of Flexible Printed Electronics Technology Center, Harbin Institute of Technology, Shenzhen 518055, China<sup>3</sup> School of Materials Science and Engineering, Anhui University, Hefei 230093, China<sup>4</sup> Faculty of Materials Science and Engineering, Shenzhen Institute of Advanced Technology, Chinese Academy of Sciences, Shenzhen 518055, China

\* Correspondence: mofunian@hit.edu.cn (F.M.); haibo@ahu.edu.cn (H.H.); gj.liang@siat.ac.cn (G.L.)

**Abstract:** Aqueous Zn-ion Batteries (AZIBs) have garnered significant interest in recent years, owing to their inherent safety, affordability, and eco-friendliness. Recently, substantial research has been conducted to broaden the application scenarios of AZIBs by regulating the electrode and electrolyte materials. In this review, we provide a comprehensive analysis of the challenges and solutions associated with AZIBs to meet extreme conditions, such as low temperatures, high temperatures, and wide temperature ranges. We also discuss electrolyte optimization strategies for each of these conditions. Finally, we outline potential avenues for further advancements and offer insights into the future of this burgeoning field of AZIBs.

**Keywords:** Zn-ion batteries; aqueous batteries; wide temperature; electrolyte engineering



**Citation:** Sun, L.; Song, Z.; Deng, C.; Wang, Q.; Mo, F.; Hu, H.; Liang, G. Electrolytes for Aqueous Zn-Ion Batteries Working in Wide-Temperature Range: Progress and Perspective. *Batteries* **2023**, *9*, 386. <https://doi.org/10.3390/batteries9070386>

Academic Editor: Hirotohi Yamada

Received: 22 June 2023

Revised: 4 July 2023

Accepted: 10 July 2023

Published: 20 July 2023



**Copyright:** © 2023 by the authors. Licensee MDPI, Basel, Switzerland. This article is an open access article distributed under the terms and conditions of the Creative Commons Attribution (CC BY) license (<https://creativecommons.org/licenses/by/4.0/>).

## 1. Introduction

In today's society, with the continuous expansion at social and economic scales, people's demand for energy and resources is growing [1–7]. Countries and regions around the world have prioritized new energy storage technologies to effectively utilize the green, low-carbon, and environmentally friendly renewable energy sources [8]. In recent years, batteries based on electrochemical energy storage are one of the most efficient, simple, and reliable devices available, and they have become the focus of research to improve their electrochemical performance and to broaden their application scenarios [2,9–13].

The aqueous Zn-based batteries are one of the most promising battery systems for large-scale storage due to their intrinsic safety and low cost by applying the H<sub>2</sub>O-based electrolyte. More importantly, the Zn metal anode could accommodate high theoretical gravimetric capacity and the volumetric capacity at 820 mAh/g and 5855 mAh/cm<sup>3</sup>, respectively, enabling it to deliver high energy and power at full cell level (Figure 1a) [14–19]. Therefore, aqueous Zn-ion batteries (AZIBs) have sparked a lot of enthusiasm in the energy storage field due to their inherent safety, low cost, and environmental friendliness [20–24].

The demand for energy storage and conversion has become diversified such that the AZIBs need to operate over a wide temperature range as global temperature extremes intensify to wide ranges [25–28]. The publication of papers on the topic of wide-temperature AZIBs in the Web of Science database since the last three years was counted (Figure 1b). The results show that the number of relevant papers published on this topic has increased year by year since the last three years, and the total number of papers published exceeded more than 2200 until the preparation of this manuscript, especially from 2020 to 2021. The growth rate of papers published has reached as much as 81.51%, indicating that many research workers in this research area have emerged in the fields of energy batteries and

material preparation. However, AZIBs face significant challenges in Zn electrode and electrolyte performance under wide-temperature operating conditions, resulting in poor battery stability and inferior electrochemical performance for a wide temperature range [29–31]. Specifically, the solidification of the aqueous electrolytes at sub-zero temperatures would result in a large decrease in the ionic conductivity of the electrolyte, thus deteriorating the poor rate capability and the large over-potentials of the working voltages for the AZIBs. In addition, the intensified protons' activity of the aqueous electrolyte would trigger severe side reactions, such as the hydrogen evolution, and accelerate the dendrite/by-products formation at high temperatures, thus deteriorating the cycling stability of the AZIBs. Consequently, developing AZIBs capable of operating under wide temperature conditions holds significant scientific and practical importance. Nevertheless, realizing excellent electrochemical performance for AZIBs under wide temperature conditions remains a considerable challenge both theoretically and technologically.

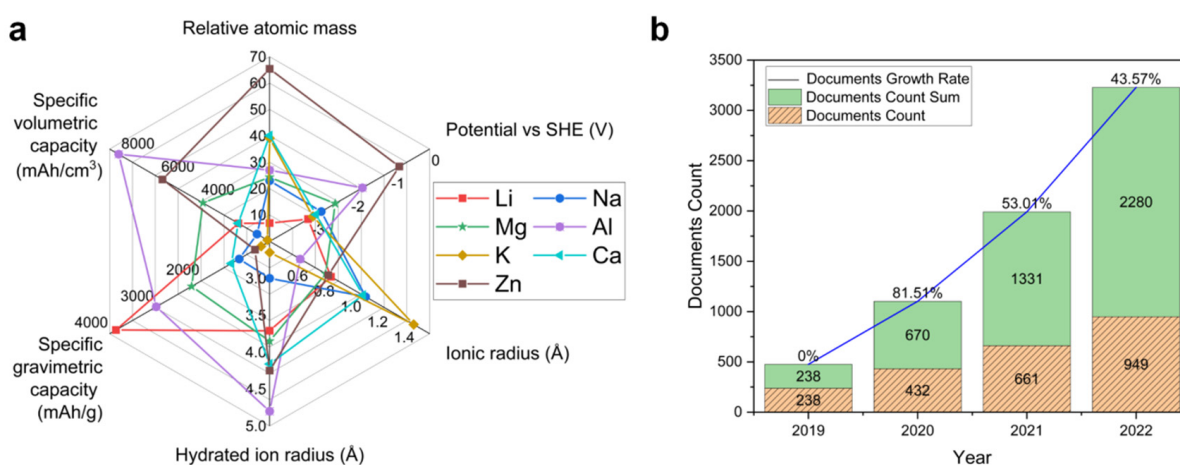


**Figure 1.** (a) Comparison of the properties of common metals used as ion batteries. (b) Statistics of papers published on the topic of wide-temperature aqueous Zn-ion batteries in the past three years.

Current studies focus on the failure mechanism and performance optimization of AZIBs to enhance their practical application under wide temperature conditions [31–38]. At present, according to the division of the working temperature range, AZIB research is mainly divided into “low temperature condition” and “high temperature condition” branches [3,39–43]. Unfortunately, few review articles have been published thus far focusing on the detailed analysis and systematic summary of electrolytes used in AZIBs operating at wide temperatures. Examining the latest progress and potential guidance to improve the wide-temperature performance of AZIBs is a compelling and necessary research frontier.

## 2. Low Temperature Condition

Energy storage batteries in certain activities, such as high latitude and polar areas, often face harsh low temperature operating environments. The solvent of AZIBs' electrolyte is based on water as  $H_2O$ ; however, the physicochemical properties of  $H_2O$  solvent at temperatures below  $0\text{ }^\circ\text{C}$  would pose numerous challenges to the stable operation of AZIBs, including electrolyte solidification, reduced ionic conductivity, and poor electrolyte-to-electrode wettability. It would inhibit the desolvation and diffusion of  $Zn^{2+}$  at the electrode/electrolyte phase interface. Preventing electrolyte solidification at subzero conditions and constructing low-temperature AZIBs is a priority [44–48].

Hydrogen bonding is the basic structural and energy storage unit of  $H_2O$  solvent. The hydrogen bonding constantly breaks and reorganizes between water molecules, forming a unique “hydrogen bonding network” structure [49–51]. The freezing process involves a complex rearrangement of the hydrogen bonding network from disordered water molecules

to ordered ice, driven by the formation of additional thermodynamic driving force. When the ambient temperature drops to 0 °C, the aqueous solution eventually forms solid ice, and the electrolyte viscosity increases until it solidifies. The freezing of the electrolyte not only decreases ionic conductivity but also reduces electrolyte-to-electrode wettability, hindering desolvation and the diffusion of Zn<sup>2+</sup> at the electrode/electrolyte phase interface. Reducing the freezing point of the electrolyte and inhibiting ice crystal formation are generally accepted as prerequisites to ensuring AZIB operation at low temperatures [25,26]. The dominant research has focused on reconstructing the hydrogen bonding network of the aqueous electrolyte by introducing effective additives.

### 2.1. Optimizing Aqueous Electrolytes

Aqueous electrolytes could serve as a medium for ionic conduction and facilitating electrochemical reactions. The properties of the electrolyte could determine the migration rate of Zn<sup>2+</sup> ions, solvation structure, electrode/electrolyte interface stability, safety, and electrochemical performance of the battery. Various strategies have been employed to design anti-freeze electrolytes, thereby enhancing AZIBs' performance at subzero temperatures, including highly concentrated electrolytes, water/organic hybrid electrolytes, and anti-freeze hydrogels. These approaches have proven to be both feasible and effective. Table 1 shows the summary of the electrochemical performance in AZIBs at low temperature.

**Table 1.** The summary of electrochemical performance in AZIBs at low temperature (anode: Zn).

Cathodes	Electrolytes	Temperature	Electrochemical Performance	Ref.
polyaniline	ZnCl <sub>2</sub>	−70 °C	85 mAh/g after 2000 cycles at 0.2 A/g	[52]
tetrachlorobenzoquinone	Zn(BF <sub>4</sub> ) <sub>2</sub>	−60 °C	86.1 mAh/g at 0.1 C	[40]
		−80 °C	71.8 mAh/g at 0.1 C	
		−95 °C	63.5 mAh/g at 0.1 C	
polyaniline	Zn(ClO <sub>4</sub> ) <sub>2</sub>	−30 °C	64 mAh/g after 2500 cycles at 5 A/g	[53]
Pyrene4,5,9,10-tetraone	Mg(ClO <sub>4</sub> ) <sub>2</sub> -Zn(ClO <sub>4</sub> ) <sub>2</sub>	−70 °C	101.5 mAh/g at 0.2 A/g	[54]
Phenazine	Mg(ClO <sub>4</sub> ) <sub>2</sub> -Zn(ClO <sub>4</sub> ) <sub>2</sub>	−70 °C	71 mAh/g at 1.2 A/g	[54]
V <sub>2</sub> O <sub>5</sub>	(Zn(OTf) <sub>2</sub> )-DOL-H <sub>2</sub> O <sup>a</sup>	−30 °C	131 mAh/g after 300 cycles at 0.1 A/g	[55]
PANI-V <sub>2</sub> O <sub>5</sub> <sup>b</sup>	EG-H <sub>2</sub> O <sup>c</sup>	−20 °C	100 mAh/g after 250 cycles at 0.2 A/g	[56]
MnO <sub>2</sub>	polyvinyl alcohol (PVA)/glycerol gel	−35 °C	25.8 mWh/cm	[57]
			732 Wh/cm	
NH <sub>4</sub> V <sub>3</sub> O <sub>8</sub> ·1.9H <sub>2</sub> O	xanthan-ZnCl <sub>2</sub>	−20 °C	201 mAh/g at 0.2 A/g	[58]
		−40 °C	83 mAh/g at 0.2 A/g	
MnO <sub>2</sub>	EG-waPUA <sup>d</sup>	−20 °C	196 mAh/g at 0.3 A/g	[59]

(a) Zn(OTf)<sub>2</sub> = Zn(CF<sub>3</sub>SO<sub>3</sub>)<sub>2</sub>; DOL = 1,3-dioxolane; (b) PANI = Polyaniline; (c) EG = ethylene glycol; (d) waPUA = waterborne anionic polyurethane acrylates.

#### 2.1.1. Water-in-Salt Electrolyte

Thermodynamically, pure water freezes at 0 °C at standard atmospheric pressure. Highly concentrated (or saturated) salt solutions, e.g., the salt-in-water electrolytes, can effectively reduce the freezing point by weakening hydrogen bonding between water molecules [25,60]. Zhang et al. [52] reported that aqueous ZnCl<sub>2</sub> electrolyte with a high concentration of 7.5 mol/L has a high ionic conductivity (1.79 mS cm<sup>−1</sup> at −60 °C) and good compatibility with the Zn anode under low temperature conditions. The solid–liquid transition temperature of the aqueous electrolyte is suppressed from 0 °C to −114 °C by disrupting the initial hydrogen bonding network in the ZnCl<sub>2</sub> solution. Based on the ZnCl<sub>2</sub> electrolyte, they created a polyaniline || Zn cell that can function in an extremely low temperature range. The specific capacity is near 85 mAh/g under the current 0.2 A/g and the long cycling performance of ~2000 cycles at −70 °C (Figure 2a). The interactions between the ions and the water molecules causes the initial hydrogen bond structure to be reconstructed, as seen in Figure 2b, and Zn<sup>2+</sup> solvation configurations appear. This electrolyte is mostly made up of Zn(H<sub>2</sub>O)<sub>2</sub>Cl<sub>4</sub><sup>2−</sup>, ZnCl<sup>+</sup>, and Zn(H<sub>2</sub>O)<sub>6</sub><sup>2+</sup>, as well as water molecules with weak hydrogen bond interactions. The electrolyte's freezing point is

reduced by the high-concentrated ions to weaken the hydrogen bond among the H<sub>2</sub>O molecules [52].

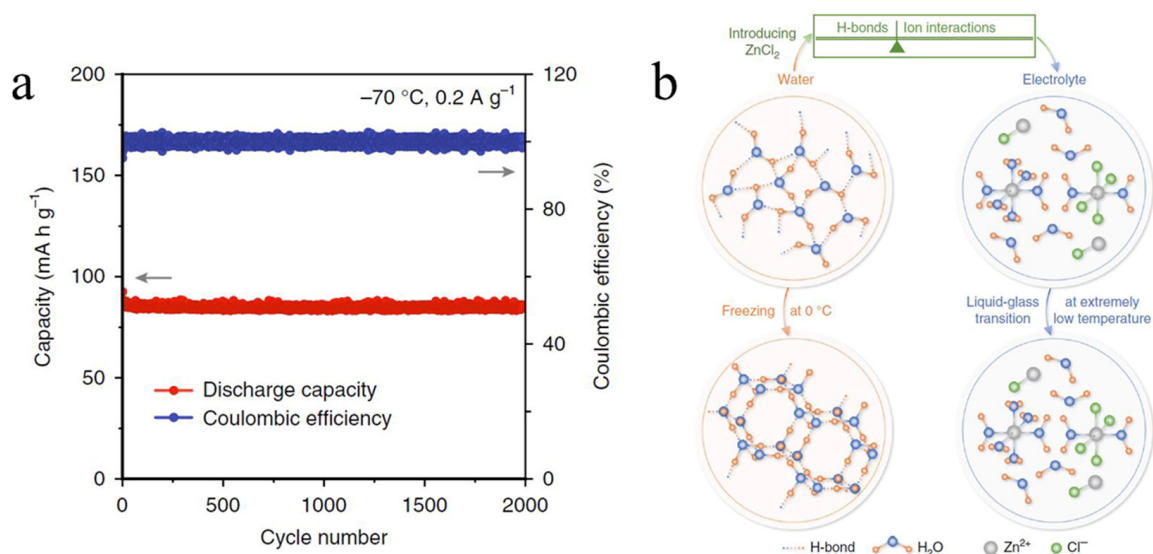


**Figure 2.** (a) Cycling performance of PANI|LTE|Zn batteries at  $-70\text{ }^{\circ}\text{C}$  at  $0.2\text{ A/g}$ . LTE = low-temperature electrolyte. (b) The schematic of the structure evolutions of water and electrolyte, and the design of low- $T_f$  solution. Original water network linked by H-bonding can easily transform to ice network at  $0\text{ }^{\circ}\text{C}$ . After adding  $\text{ZnCl}_2$ , the H-bond network is broken by the strong interaction between ions and water, while the ion interactions are enhanced. By balancing the H-bonding and ion interactions for modulating  $T_f$ , the electrolyte at critical  $C_{\text{ZnCl}_2}$  can be operated at extremely low temperature. © Copyright 2020, The Author(s) [52].

It is worth mentioning that Sun et al. [40] introduced the  $\text{BF}_4^-$  anions to break the original hydrogen bonding network between H<sub>2</sub>O molecules by forming O-H...F hydrogen bonding and developed a  $\text{Zn}(\text{BF}_4)_2$  electrolyte with a low freezing point ( $-122\text{ }^{\circ}\text{C}$ ) and high ionic conductivity. The Zn||tetrachlorobenzoquinone (TCBQ) cell based on the 4 mol/L  $\text{Zn}(\text{BF}_4)_2$  electrolyte exhibited excellent electrochemical performance over a low temperature range from  $-60\text{ }^{\circ}\text{C}$  to  $-95\text{ }^{\circ}\text{C}$ . The Zn/TCBQ battery achieves a high discharge specific capacity of 86.1 mAh/g, 71.8 mAh/g, and 63.5 mAh/g at  $-60\text{ }^{\circ}\text{C}$ ,  $-80\text{ }^{\circ}\text{C}$ , and  $-95\text{ }^{\circ}\text{C}$ , respectively, at an average voltage of 1.2 V. It has been shown that adding  $\text{BF}_4^-$  anions could damage the hydrogen bond (HB) network in water molecules and reduce the freezing point even further. To study the development of HBs in this system from a basic perspective, molecular dynamics (MD) simulations were used. The pictures in Figure 3a,b [40] clearly show that following the addition of 4 M  $\text{Zn}(\text{BF}_4)_2$  salt, the HBs of water molecules have rapidly diminished, and a large number of O-H...F HBs among  $\text{BF}_4^-$  ions and water molecules are generated. Four different forms of HBs among water molecules and the  $\text{BF}_4^-$  anion have been identified from the outcomes of MD simulations, and they are shown in Figure 3c–f. The mean number of hydrogen bonding between  $\text{BF}_4^-$  ions and water molecules is shown in Figure 3g. In Figure 3h, the ratio of the various kinds of HBs is shown. With an increase in  $\text{Zn}(\text{BF}_4)_2$  quantity, the ratio of O-H...O HBs steadily declines. In contrast, all HB ratios show a trend to decline, and the proportion of O-H...F HBs gradually rises, demonstrating that the addition of  $\text{BF}_4^-$  ions not only disrupts the HB network but also decreases the amount of HBs present in the initial water molecules [40].

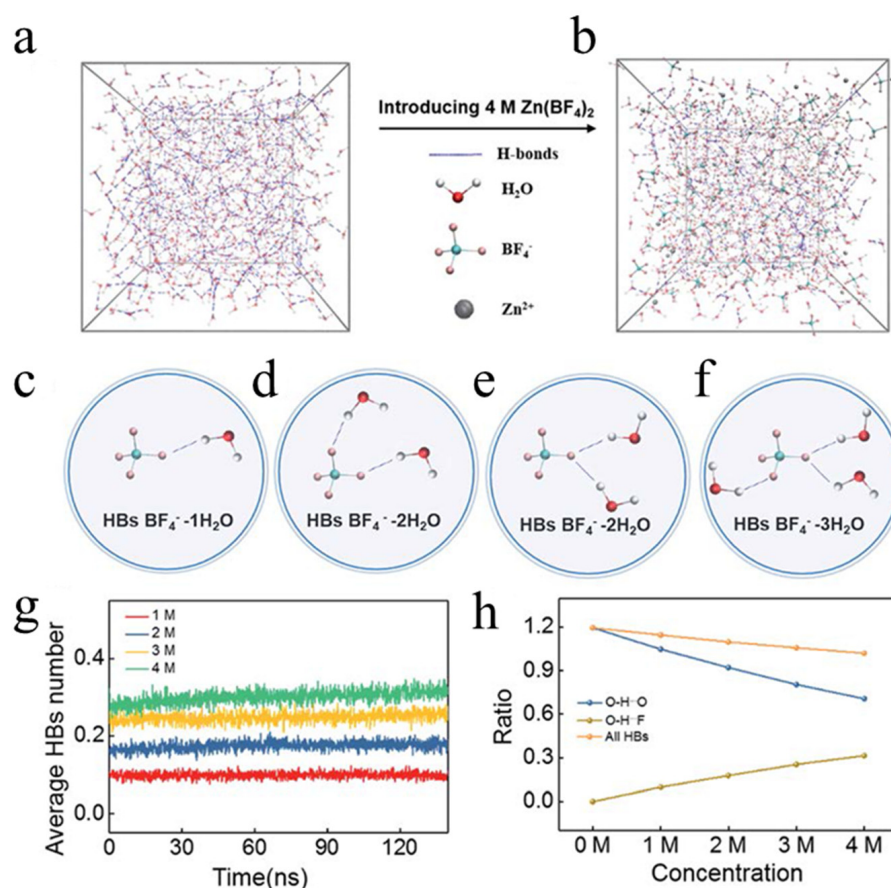


**Figure 3.** (a) Snapshot of the MD simulation of water. The dashed blue line represents the HBs. (b) Snapshot of the MD simulation of 4 M  $\text{Zn}(\text{BF}_4)_2$  electrolyte. (c–f) Different types of O–H···F HBs from the snapshot. (c)  $\text{BF}_4^- \cdot 1\text{H}_2\text{O}$ . (d)  $\text{BF}_4^- \cdot 2\text{H}_2\text{O}$ . (e)  $\text{BF}_4^- \cdot 2\text{H}_2\text{O}$ . (f)  $\text{BF}_4^- \cdot 3\text{H}_2\text{O}$ . (g) Average HB numbers for each system after 140 ns simulation time. (h) The ratio of different HBs. © Copyright 2021, The Royal Society of Chemistry [40].

The reports above greatly provide an effective strategy to promote low-temperature AZIBs by adjusting the electrolyte structure with highly concentrated solutions of salt. Although “water-in-salt” electrolytes have significant advantages, such as lower electrolyte freezing point and improved electrode materials, it is still a fundamental challenge to overcome the inherent limitations of “water-in-salt” electrolytes in the future, including high viscosity caused by strong cation–anion coupling, high cost, and salt precipitation at low temperature. Therefore, excessive salt concentrations might be optimized when designing anti-freezing electrolytes, and the development of low-cost salt for highly concentrated electrolyte is essential to improve market competitiveness.

### 2.1.2. Organic Additives

Introducing organic additives into the aqueous electrolytes is a key strategy to realize the low freezing points of the electrolyte. The effectiveness of additives to expand the low-temperature range of AZIBs largely relies on the capabilities to disturb and reconstruct the hydrogen bond network to inhibit the regular formation of ice crystals, and thus reduce the freezing point of the electrolyte. At present, a large number of organic solvents have been applied to reduce the freezing point of the electrolytes for AZIBs, such as 1,3-Dioxolane (DOL) [55], ethylene glycol (EG) [61–64], ethanol [65], and glycerol [66,67].

1,3-Dioxolane (DOL), an organic solvent with a low freezing point and a high dielectric constant, is an exemplified solvent as an additive in aqueous electrolytes. Du et al. [55] reported a “Zn trifluoromethanesulfonate ( $\text{Zn}(\text{OTf})_2$ )-DOL- $\text{H}_2\text{O}$ ” electrolyte to reduce

the freezing point of the electrolyte to  $-51.2\text{ }^{\circ}\text{C}$ , which enabled the  $\text{Zn}|\text{V}_2\text{O}_5$  cell to maintain  $131\text{ mA/g}^{-1}$  at a low temperature of  $-30\text{ }^{\circ}\text{C}$ . This enables the  $\text{Zn}|\text{V}_2\text{O}_5$  cell to maintain a stable average capacity of  $131\text{ mAh/g}$  for 300 cycles at  $0.1\text{ A/g}$  current density at a low temperature of  $-30\text{ }^{\circ}\text{C}$  (Figure 4a). To further study the interaction between the components in the mixed electrolyte, the solvation structure of the aqueous electrolyte and the 1:1 electrolyte was studied by MD simulation. For the 1:1 electrolyte, the snapshot of the simulated electrolyte structure shows that the DOL molecule is combined with the  $\text{H}_2\text{O}$  molecule by hydrogen bonding (Figure 4b,c). There are two forms of binding between DOL and  $\text{H}_2\text{O}$ . Most DOL interacts with only one  $\text{H}_2\text{O}$  molecule, and some DOL binds to two  $\text{H}_2\text{O}$  molecules. The probabilities of DOL- $\text{H}_2\text{O}$ , DOL-2 $\text{H}_2\text{O}$ , and  $\text{H}_2\text{O}$ - $\text{H}_2\text{O}$  were calculated by the Density Function Theory (DFT). As shown in Figure 4d, the binding energies of DOL- $\text{H}_2\text{O}$  and DOL-2 $\text{H}_2\text{O}$  are  $2.662\text{ kcal/mol}$  and  $5.278\text{ kcal/mol}$ , respectively, and the binding energies of  $\text{H}_2\text{O}$ - $\text{H}_2\text{O}$  are  $2.542\text{ kcal/mol}$ , respectively. The theoretical calculation results further prove that  $\text{H}_2\text{O}$  is more inclined to combine with DOL than  $\text{H}_2\text{O}$  [55].

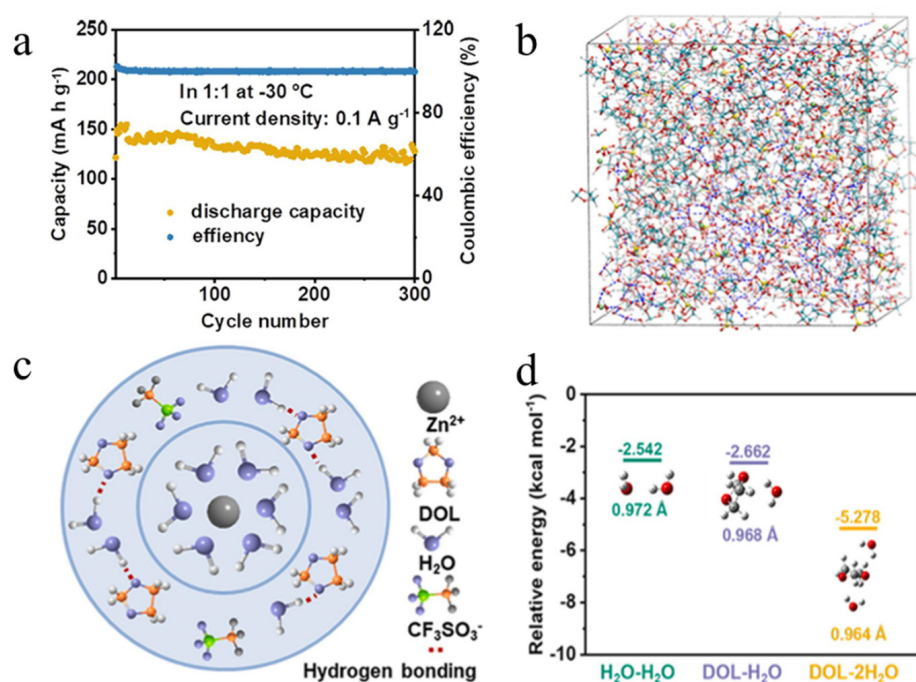


**Figure 4.** (a) Cycling stability of  $\text{ZnV}_2\text{O}_5$  cell based on the hybrid electrolyte at  $-30\text{ }^{\circ}\text{C}$  with a current density of  $0.1\text{ A/g}$ . (b) Snapshot of the MD simulation cell for the 1:1 electrolyte. (c) The solvation structure of  $\text{Zn}^{2+}$  obtained by MD simulation. (d) Relative binding energy for DOL with  $\text{H}_2\text{O}$  molecules obtained from DFT calculations. © Copyright 2021, Elsevier B.V [55].

The “Zn sulfate ( $\text{ZnSO}_4$ )-EG- $\text{H}_2\text{O}$ ” electrolyte designed by Chang et al. has high ionic conductivity at low temperature. The research [56] shows that the  $\text{Zn}^{2+}$ -EG solvation effectively reduces the freezing point of the mixed electrolyte, improves the reversibility of Zn deposition/stripping, and improves the deposition morphology of the Zn anode. Therefore, the  $\text{Zn}/\text{PANI-V}_2\text{O}_5$  battery with EG40 (volume ratio of EG to water is 40%) exhibits high discharge capacity of  $100\text{ mAh/g}$  at  $0.2\text{ A/g}$  current density and long cycle life (250 cycles) at  $-20\text{ }^{\circ}\text{C}$  (Figure 5a). To further study the solvation structure of a mixed electrolyte, MD simulation and DFT calculation were carried out. The snapshots of the simulated electrolyte structure (Figure 5b,c) show that there are ionic solvation clusters of  $\text{Zn}^{2+}$  coordinated with  $\text{SO}_4^{2-}$ ,  $\text{H}_2\text{O}$ , and EG in the electrolyte with EG addition. The coordination number (CN) analysis of  $\text{H}_2\text{O}$ , EG, and  $\text{SO}_4^{2-}$  around  $\text{Zn}^{2+}$  in a series of hybrid electrolytes is shown in Figure 5d. With the increasing EG-to-water ratio, the CN of  $\text{SO}_4^{2-}$  anions around  $\text{Zn}^{2+}$  increased slightly. The CN of  $\text{H}_2\text{O}$  molecules in the first hydration layer gradually decreased, while the CN of EG molecules gradually increased,

indicating that the introduction of EG greatly destroyed the solvation structure of  $\text{Zn}^{2+}$  and  $\text{H}_2\text{O}$ . With the increasing EG content, the diffusion coefficient of  $\text{Zn}^{2+}$  increased first and then decreased (Figure 5e). When the ratio of EG-to-water is less than 60%, the diffusion coefficient of the mixed electrolyte is still higher than that of EG0. This indicates that the solvation structure of  $\text{Zn}^{2+}$  coordinated with EG and  $\text{H}_2\text{O}$  contributes to the rapid transport of  $\text{Zn}^{2+}$ . Nevertheless, when the solvation effect of EG and  $\text{Zn}^{2+}$  is more prominent, the  $\text{Zn}^{2+}$  in the mixed electrolyte achieved rapid transport at low temperature. In addition, the relative binding energies of  $\text{Zn}^{2+}$  cations with anions and solvents are in the order of  $\text{Zn}^{2+}\text{-SO}_4^{2-} > \text{Zn}^{2+}\text{-EG} > \text{Zn}^{2+}\text{-H}_2\text{O}$ . The results show that  $\text{Zn}^{2+}$  is preferentially coordinated with EG rather than  $\text{H}_2\text{O}$ , resulting in the rapid exchange of EG around  $\text{Zn}^{2+}$ , so that  $\text{Zn}^{2+}$  is rapidly conductive in the electrolyte added with EG. In addition, after the introduction of EG molecules in the system, the electrostatic potential of the solvation state of  $\text{Zn}^{2+}\text{-5H}_2\text{O}$  (Figure 5f,g) was significantly reduced. Therefore, the electrostatic repulsion between  $\text{Zn}^{2+}$  cations can be reduced.

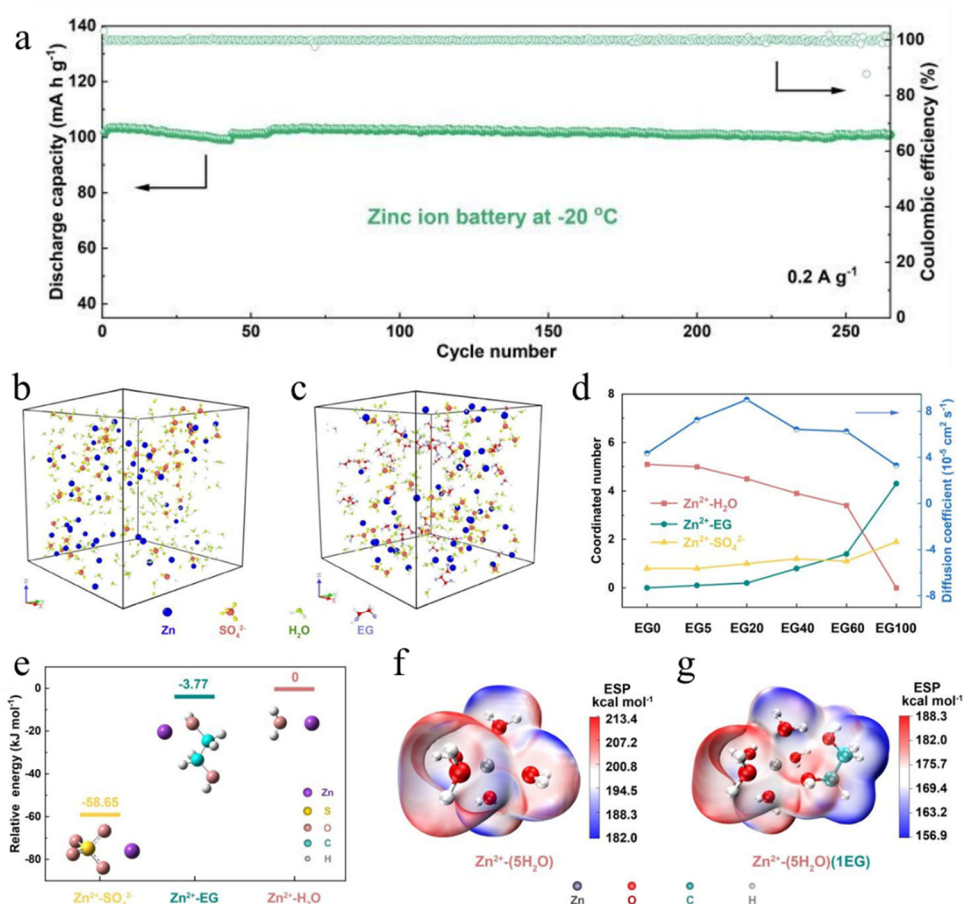


**Figure 5.** (a) Low-temperature performance of ZnPANI-V<sub>2</sub>O<sub>5</sub> batteries based on EG40 at  $-20\text{ }^\circ\text{C}$  with a current density of  $0.2\text{ A/g}$ . (b–g) Optimized structure for the hybrid electrolytes from MD simulations and DFT calculations. Snapshots of (b) EG0 and (c) EG40 during MD simulations. (d) Coordinated numbers of H<sub>2</sub>O, EG, and SO<sub>4</sub><sup>2-</sup> around Zn<sup>2+</sup> and the diffusion coefficient of Zn<sup>2+</sup>-indifferent electrolytes calculated from MD simulations. (e) Relative binding energy for Zn<sup>2+</sup> with different species obtained from DFT calculations. Electrostatic potential maps of (f) the original Zn<sup>2+</sup>-H<sub>2</sub>O system and (g) the EG-added system. © Copyright 2020, The Royal Society of Chemistry [56].

In general, organic solvents possessing certain attributes, such as low melting points, reduced viscosity, and elevated polarity, can effectively decrease electrolyte freezing points and suppress water-induced side reactions. Although implementing organic electrolyte systems enhances electrochemical stability at subzero temperatures, capacity or voltage may

be compromised [68,69]. Notably, the majority of the organic solvents exhibit flammability and toxicity, which may pose safety concerns when present in excess within hybrid electrolytes. Consequently, the design of water/organic hybrid electrolytes for low-temperature applications should judiciously minimize the incorporation of superfluous organic solvents.

### 2.1.3. Hydrogel Electrolyte

The hydrogels emerge as a promising solution to enable the working capability for AZIBs to work at sub-zero temperatures. Hydrogels are cross-linked hydrated polymer chains rich in hydrophilic functional groups, such as -OH, -COOH, -SO<sub>3</sub>, and -NH<sub>2</sub>. The formation of intra- or intermolecular hydrogen bonding within hydrogels, as well as the competition between water molecules across different chemical functional groups, regulates their anti-freeze properties.

Hydrogel electrolytes offer enhanced electrode interface stabilization compared to liquid electrolytes [70] and are frequently utilized in conjunction with co-solvents, additives, or highly concentrated salts to extend their low-temperature performance [71]. Chen et al. [57] developed a frost-resistant borax cross-linked polyvinyl alcohol (PVA)/glycerol gel electrolyte capable of withstanding temperatures below -60 °C. Employing this anti-freeze gel electrolyte, they constructed a stretchable quasi-solid-state Zn-MnO<sub>2</sub> battery with an energy density of 46.8 mWh/cm<sup>3</sup> (1330 Wh/cm<sup>2</sup>) at 25 °C and a power density of 96 mW/cm<sup>3</sup> (2.7 mW/cm<sup>2</sup>), surpassing nearly all reported AZIBs (Figure 6a,b). More importantly, even at -35 °C, it can still reach a relatively high energy density (25.8 mWh/cm<sup>3</sup>, 732 Wh/cm<sup>2</sup>). When the power density increases by about 10 times, it can maintain 53.3% of the energy density.

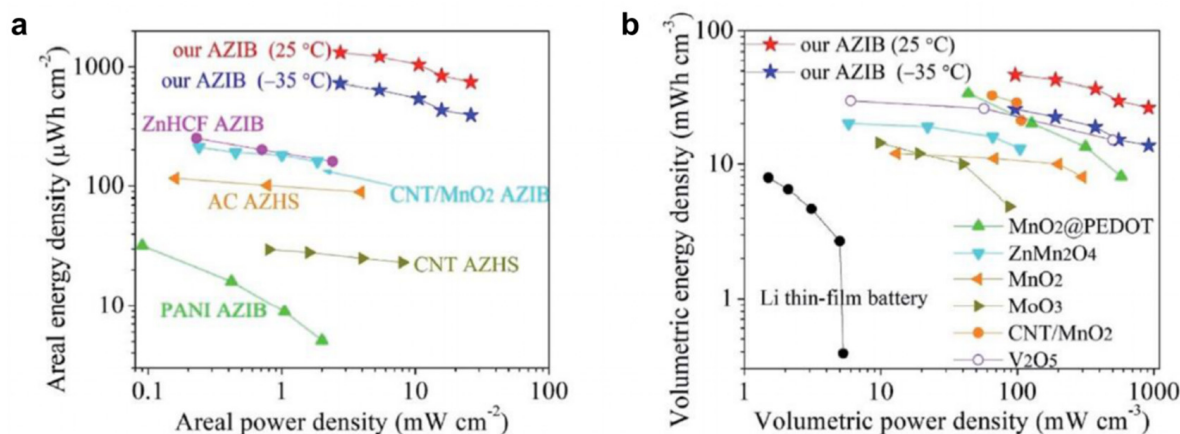


**Figure 6.** AZIB performance using hydrogel electrolyte. (a) Areal and (b) volumetric Ragone plots of our PVA-B-G battery, in comparison with previously reported energy storage devices. © Copyright 2020, The Royal Society of Chemistry [57].

Wang et al. [58] devised a concentrated hydrogel electrolyte by combining xanthan gum with a ZnCl<sub>2</sub> aqueous solution, forming a hydrogel electrolyte. At -20 °C and -40 °C, the discharge-specific capacities were 201 mAh/g and 83 mAh/g, respectively, when the current density was 0.2 A/g (Figure 7a,b). An ethylene glycol (EG)-based aqueous anionic polyurethane acrylate (EG-waPUA) hydrogel electrolyte was employed in a flexible Zn/MnO<sub>2</sub> battery. H<sub>2</sub>O molecules are confined through effective hydrogen bond interactions with EG and polymer molecules, enabling the freezing point to be controlled by adjusting the EG content. The hydrogel remains unfrozen at -20 °C when the EG content reaches a certain threshold. The optimized hydrogel retains an ionic conductivity of 14.6 mS/cm and exhibits robust mechanical properties at -20 °C. Furthermore, the Zn-MnO<sub>2</sub> battery assembled with this gel electrolyte demonstrates exceptional low-temperature performance, retaining over 80% of its capacity when transitioning from room temperature to -20 °C. No significant capacity degradation was observed after several alternating cycles between high and low temperatures (Figure 7c) [59].

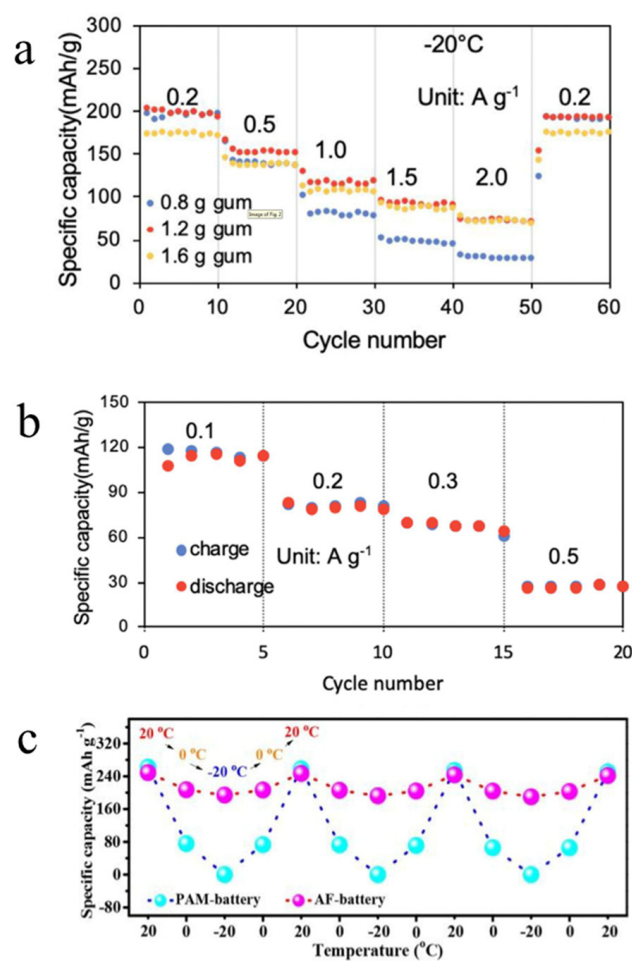


**Figure 7.** (a) Rate of electrochemical performance of the batteries based on the electrolytes prepared using 0.8 g, 1.2 g, and 1.6 g of xanthan gum combined with 4 m  $\text{ZnCl}_2$  at  $-20^{\circ}\text{C}$ . © Copyright 2021, Elsevier Ltd. [58]. (b) Rate performance of the battery with the optimized electrolyte at  $-40^{\circ}\text{C}$ . © Copyright 2021, Elsevier Ltd. [58]. (c) Cyclic testing of PAM-battery and AF-battery under 20, 0,  $-20^{\circ}\text{C}$  at 0.3  $\text{A/g}$ . PAM = polyacrylamide; AF = anti-freezing. © Copyright 2019, The Royal Society of Chemistry [59].

Huang et al. [53] form ternary and weak hydrogen bonding by introducing the chaotropic  $\text{ClO}_4^-$  polymer chains into the  $\text{H}_2\text{O}$  molecule network, which can reduce the freezing point of the electrolyte. Firstly, density functional theory (DFT) was used to examine how the chaotropic  $\text{ClO}_4^-$  anions, water, and polymer chains interacted. The strong retaining capacity of the hydrogel is confirmed by Figure 8a, which shows that the binding energy of PAM to water is significantly greater than that of water to water. To test the effectiveness of the  $\text{Zn}(\text{ClO}_4)_2$  salts on gel electrolyte anti-freezing, a dual-network hydrogel (designated as CSAM) composed of modified polysaccharides carboxymethyl chitosan (CMCS) and polyacrylamide (PAM) was created and used as an example system. It proves that the  $\text{ClO}_4^-$  anion has a potent interaction with PAM chains, allowing it to enter the polymer chains, break the HB in PAM-PAM and PAM-CSAM, and control the hydrogel's mechanical flexibility. This increases the hydrophilic property of the hydrogel and improves its mechanical characteristics by forming a ternary HB reciprocity between the  $\text{ClO}_4^-$  anion, water, and polymer chains, as shown in Figure 8b. Ref. [53] At  $-30^{\circ}\text{C}$ , the  $\text{Zn}/$  polyaniline battery is composed of the electrolyte with an ionic conductivity of 7.8  $\text{mS/cm}$  and a reversible capacity of 70  $\text{mAh/g}$  after 2500 cycles at a current density of 5  $\text{A/g}$  (Figure 8c).

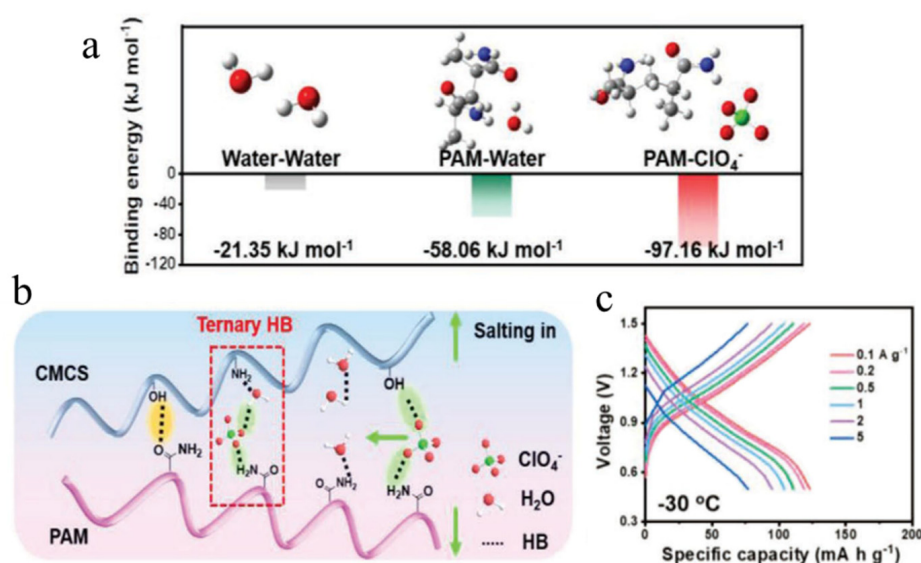


**Figure 8.** (a) DFT-optimized structures in the CSAM-C hydrogel. (b) Schematic diagram of the interactions among CMCS, ClO<sub>4</sub><sup>-</sup>, and PAM chains in CSAM-C hydrogel. (c) Rate performances of Zn/PANI battery with CSAM-C hydrogel electrolyte under −30 °C. © Copyright 2022, Wiley-VCH GmbH [53].

The performance of AZIBs at low temperatures significantly impacts their practical applications. Currently, research in this area remains in its nascent stages. Efforts to enhance the subzero temperature performance of AZIBs predominantly focus on the meticulous design of electrolytes. It is crucial to recognize that both electrode and non-active materials influence the low-temperature performance of AZIBs. Consequently, the development of anti-freezing electrolytes must consider the electrochemical stability window and ensure compatibility with both electrode and non-active materials. Additionally, the enhancement of electrolytes would generally necessitate the utilization of high-concentration salt solutions and organic electrolytes. To maintain the competitiveness of AZIBs in the market, it is essential to prioritize their cost effectiveness and their safety advantages.

### 3. High Temperature Condition

In addition to low-temperature conditions, AZIBs often encounter elevated temperatures exceeding 40 °C in various applications, such as geological exploration and deployment in tropical regions. Current research indicates that high-temperature environments can accelerate the internal chemical reaction rates, enhancing the charge transfer kinetics to a degree. At these elevated internal temperatures, solvent evaporation and solute precipitation from the electrolyte may occur, subsequently degrading the high-temperature electrochemical performance of AZIBs and potentially resulting in battery failure [72]. The issues are located at the Zn anode side corresponding to irreversible dendrites and the hydrogen evolution at high temperatures, which could be ascribed to the enhanced proton/H<sub>2</sub>O activity in the aqueous electrolyte. It would not only promote the hydrogen evolution but also accelerate the Zn dendrite formation. Furthermore, the cathode material may exhibit substantial dissolution phenomena under high-temperature conditions, leading to rapid battery capacity degradation [73]. Considering the boiling point of the aqueous solution, current research posits that increasing the electrolyte's boiling point and developing high-temperature-resistant cathode materials are fundamental requirements to ensure AZIBs' operational stability under high-temperature conditions. In this review, we specifically emphasize optimization strategies for electrolytes in AZIBs to improve their performance at elevated temperatures. Table 2 shows the summary of electrochemical performance in AZIBs at high temperature.

**Table 2.** The summary of electrochemical performance in AZIBs at high temperature (anode: Zn).

Cathodes	Electrolytes	Temperature	Electrochemical Performance	Ref.
MnO <sub>2</sub>	bentonite-colloidal	55 °C	114.9 mAh/g after 300 cycles at 2 A/g	[74]
LVO-250 <sup>a</sup>	ZnSO <sub>4</sub>	50 °C	232 mAh/g after 500 cycles at 5 A/g 192 mAh/g after 1000 cycles at 10 A/g	[75]
Te	Zn(OTf) <sub>2</sub> -H <sub>2</sub> O/PD <sup>b</sup>	100 °C	195.7 mAh/g <sub>Te</sub> after 100 cycles at 2 C (850 mA/g <sub>Te</sub> )	[43]
CuVO <sup>c</sup>	PNMT <sup>d</sup>	60 °C	200 mAh/g after 1200 cycles at 5A/g	[76]
phenanthrenequinone macrocylic trimer	ZnSO <sub>4</sub> /H <sub>2</sub> O-50% EG	60 °C	88 mAh/g after 900 cycles at 0.2 A/g	[77]
polytriphenylamine	Zn-TFMS/ (TEP:PC = 1:2) <sup>e</sup>	60 °C	300 cycles at 2 A/g	[78]

(a) LVO = Li<sub>x</sub>V<sub>2</sub>O<sub>5</sub>·nH<sub>2</sub>O; 250 = 250 °C; (b) Zn(OTf)<sub>2</sub> = Zn(CF<sub>3</sub>SO<sub>3</sub>)<sub>2</sub>; PD = 1,5-pentanediol; (c) CuVO = copper vanadate; (d) PNMT hydrogel is synthesized by free radical polymerization. Radical polymerization was used to synthesize the hydrogel with a semi-interpenetrating network with acrylamide (AM) as the monomer, TCCP with the main role of thermochromism, CNF and CMC as additives, APS as an initiator, and NNMBA as a cross-linking agent. TCCP = thermochromic capsule powder; CNF = cellulose nanofibrils; CMC = carboxymethyl cellulose IV; APS = ammonium persulfate; NNMBA = N,N'-methylenebis (acrylamide); (e) Zn-TFMS = Zn trifluoromethanesulfonate; TEP = triethyl phosphate; PC = propylene carbonate.

### 3.1. Optimizing Aqueous Electrolytes

The current AZIBs encounter various side reactions caused by water on the anode side, such as hydrogen evolution reaction, Zn corrosion, and dissolution of cathode materials, which could be ascribed to the enhanced activity of H<sup>+</sup> and H<sub>2</sub>O at high temperatures [79–83]. Consequently, inhibiting the H<sub>2</sub>O activity at high temperature could enable the stable performance of AZIBs. Recent studies have demonstrated that employing polymer and cosolvent electrolytes can suppress these undesirable side reactions [84–89]. However, to satisfy more stringent application demands, it is essential to explore further possibilities for AZIBs at elevated temperatures, potentially reaching the boiling point of water.

#### 3.1.1. Cosolvent Electrolytes

Introducing a crowding agent into the electrolyte can enhance the battery stability by suppressing parasitic reactions of the Zn metal anode at high temperatures. Wang et al. [43] achieved uniform Zn deposition at elevated temperatures using an eco-friendly crowding agent, 1,5-pentanediol (PD), which effectively reduced water reactivity and diminished H<sub>2</sub>O content in the Zn<sup>2+</sup> dissolution sheath, thereby significantly inhibiting water-induced parasitic reactions. After 100 cycles at 100 °C, the Zn//Te battery retained a discharge capacity of 195.7 mAh/g<sub>Te</sub> at 2 C (850 mA/g<sub>Te</sub>), exhibiting remarkable cycling stability under exceptionally high temperatures (Figure 9a). MD simulation can provide a more in-depth understanding of the solvation structure and intermolecular interactions of electrolytes. The basis distribution functions (RDF) of different electrolytes at 25 °C (Figure 9b,c) show that PD emits a large amount of H<sub>2</sub>O in the Zn<sup>2+</sup> solvation sheath of the Zn(OTf)<sub>2</sub>-H<sub>2</sub>O/PD electrolyte, and the Zn-O (H<sub>2</sub>O) coordination number of the Zn(OTf)<sub>2</sub>-H<sub>2</sub>O electrolyte is significantly reduced from 5.0 (83.7%) to 1.8 (29.2%) (Figure 9d), which is beneficial to suppress the parasitic side reactions caused by H<sub>2</sub>O molecules in the Zn<sup>2+</sup> solvation sheath. In addition, the change of RDF at 100 °C (Figure 9e,f) is consistent with that at 25 °C. In addition, the hydroxyl distribution of the PD isomer 1,2-pentanediol (1,2-PD) on the carbon chain is completely different (Figure 10a,b), and its application potential in high-temperature ZMBs is also studied. The H<sub>2</sub>O/1,2-PD cosolvent electrolyte was simulated by MD (Figure 10c,d). The results show that in H<sub>2</sub>O/1,2-PD, the amount of H<sub>2</sub>O in the Zn<sup>2+</sup> solvation shell is larger than that in H<sub>2</sub>O/PD, which may be due to the larger steric hindrance of the coordination between the hydroxyl group and Zn<sup>2+</sup>, thus hindering the inhibition of side reactions on the Zn anode. In addition, at 100 °C, the coulombic efficiency (CE) of the Zn/Ti battery based on H<sub>2</sub>O/1,2-PD is lower than that of the similar battery based on H<sub>2</sub>O/PD (Figure 10e), which is consistent with the MD simulation results, indicating the importance of the solvent molecular structure to the electrolyte performance.

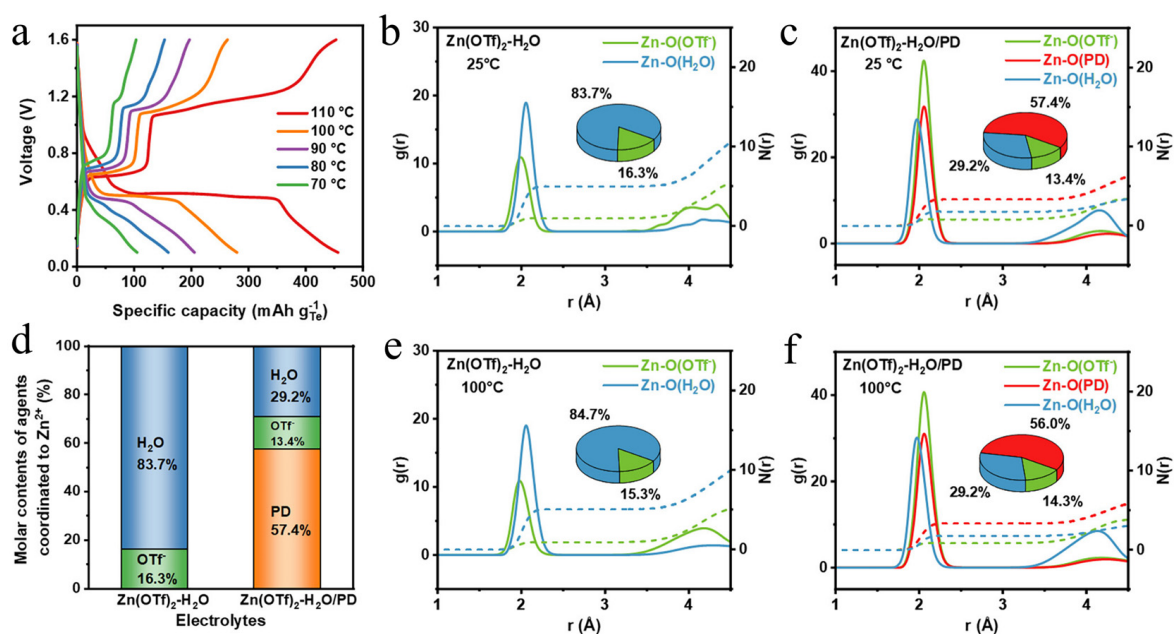


**Figure 9.** (a) Voltage profiles of ZnTe batteries with Zn(OTf)<sub>2</sub>-H<sub>2</sub>O/OPD electrolytes at temperatures ranging from 70 to 110 °C. (b,c,e,f) RDFs of the agents coordinated to Zn<sup>2+</sup> in (b,e) Zn(OTf)<sub>2</sub>-H<sub>2</sub>O electrolyte and (c,f) Zn(OTf)<sub>2</sub>-H<sub>2</sub>O/OPD electrolyte at (e,f) 25 °C and (h,i) 100 °C. (d) Ratio of different agents coordinated to Zn<sup>2+</sup> in Zn(OTf)<sub>2</sub>-H<sub>2</sub>O and Zn(OTf)<sub>2</sub>-H<sub>2</sub>O/OPD electrolytes at 25 °C. © Copyright 2022, American Chemical Society [43].

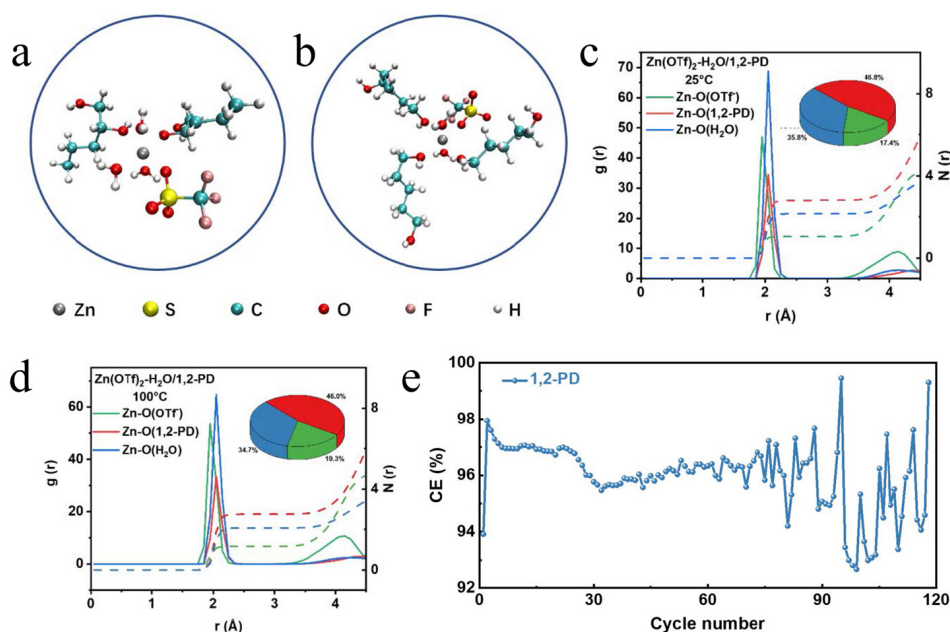


**Figure 10.** The typical configurations of the molecules in (a) Zn(OTf)<sub>2</sub>-H<sub>2</sub>O/1,2-PD and (b) Zn(OTf)<sub>2</sub>-H<sub>2</sub>O/OPD co-solvent electrolytes. The RDFs of the agents coordinate to Zn<sup>2+</sup> in Zn(OTf)<sub>2</sub>-H<sub>2</sub>O/1,2-PD electrolyte at (c) 25 °C and (d) 100 °C. (e) CE of Zn//Ti batteries with Zn(OTf)<sub>2</sub>-H<sub>2</sub>O/1,2-PD electrolytes at 1 mA cm<sup>-2</sup> and 0.5 mAh cm<sup>-2</sup> under 100 °C. © Copyright 2022, American Chemical Society [43].

Wang et al. reported a Zn-organic battery with ZnSO<sub>4</sub>/H<sub>2</sub>O-50% EG as the electrolyte and phenanthrenequinone macrocyclic trimer (PQ-MCT) as the cathode, which showed that the discharge capacities at 0.2 A/g still maintained 88 mAh/g after 900 cycles at 60 °C. In Ref. [77], Qiu et al. also reported a Zn//polytriphenylamine composite (PTPan) battery

using Zn trifluoromethanesulfonate (Zn-TFMS) salt-mixed solvent of propylene carbonate (PC) and triethyl phosphate (TEP) as the electrolyte, which maintained 300 cycles at 2 A/g at the same temperature, 60 °C. In Ref. [78], the rate performance of the PTPAn cathode at a high temperature of 60 °C and the cyclic stability of Zn//PTPAn cells at 60 °C are shown in Figure 11a,b. According to the scheme (Figure 11c), during the charging process, one of the TPA units (containing a C-N bond) at first gives up one p-electron of the C=N bond and then becomes positively charged, producing the corresponding radical cation (C=N<sup>+</sup>) and anion TDMS<sup>-</sup> and attracting p-electrons from the benzene ring under the connection of intermolecular forces, while the second adjacent TPA loses another electron of C=N bond at higher potential. Therefore, the reaction at the PTPAn cathode includes the oxidation/reduction of the TPA units (i.e., C-N $\rightleftharpoons$  C=N<sup>+</sup>) and is accompanied by the combination/release of the TFMS into the polymer chains.

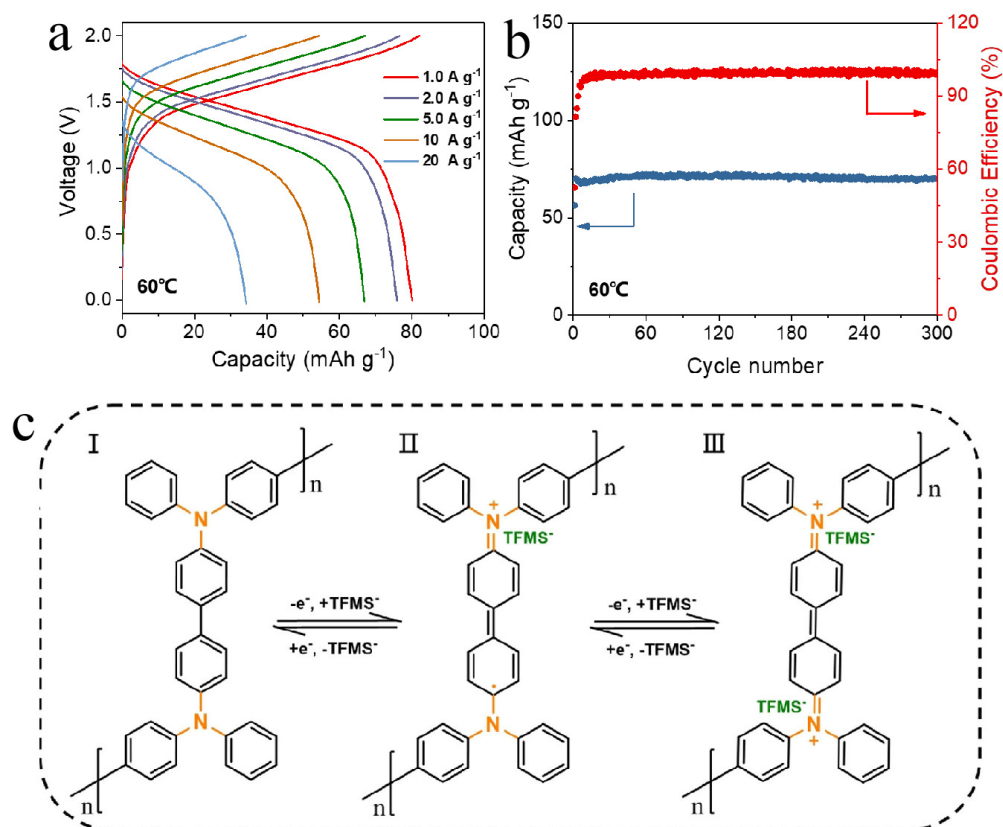


**Figure 11.** (a) The rate performance of PTPAn cathode at high temperature of 60 °C and (b) cyclic stability of Zn//PTPAn cells at 60 °C was shown. (c) Scheme showing the reactions at the PTPAn cathode. © Copyright 2021, Wiley-VCH GmbH [78].

### 3.1.2. Colloidal Electrolytes

Colloidal electrolytes have been reported to enhance the high-temperature electrochemical performance of AZIBs positively. Xie et al. [74] proposed a high-temperature-resistant “Ben-colloid” colloidal electrolyte, prepared by mixing liquid electrolyte (2 M ZnSO<sub>4</sub> and 0.1 M MnSO<sub>4</sub>) with bentonite. AZIBs assembled using this colloidal electrolyte maintained a capacity of 114.9 mAh/g after 300 cycles at a current density of 2 A g<sup>-1</sup> at 55 °C (Figure 12a). Yang et al. reported that a cotton-like LVO-250 battery using ZnSO<sub>4</sub> electrolyte showed excellent electrochemical performance with 232 mAh/g after 500 cycles at 5 A/g, and 192 mAh/g after 1000 cycles at 10 A/g at 50 °C [75].

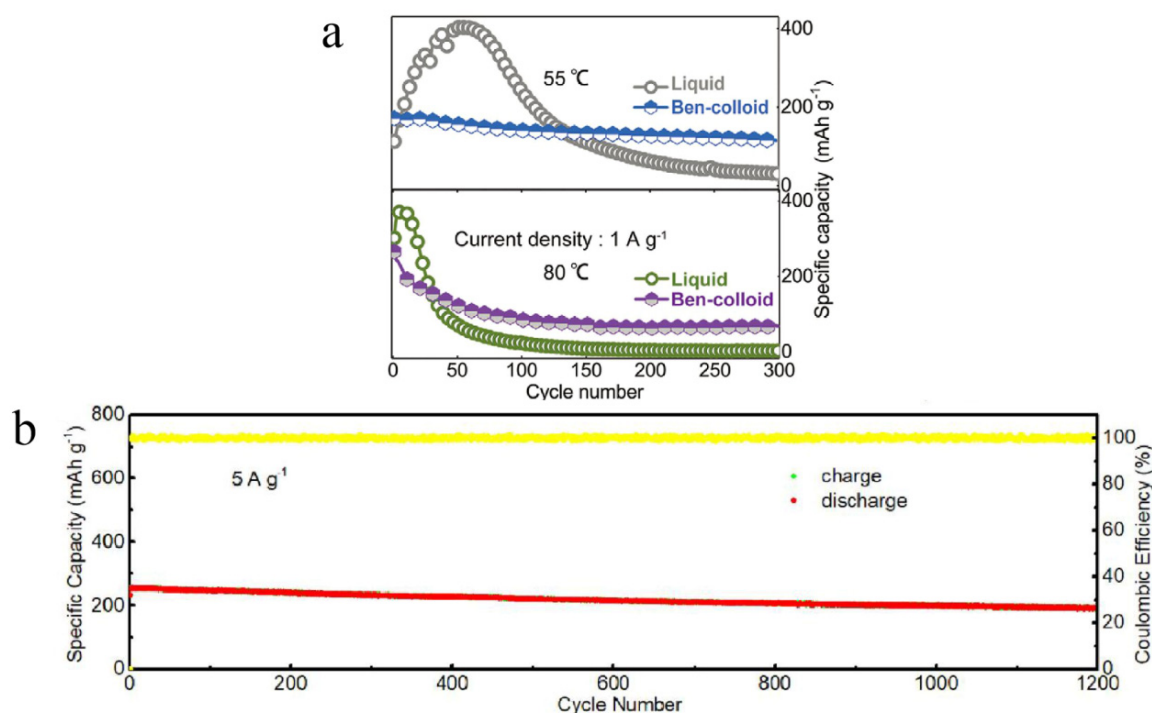


**Figure 12.** AZIB performance at high temperature condition. (a) The function of ben-colloid electrolyte and electrochemical performance at 55 and 80 °C. © Copyright 2021, Wiley-VCH GmbH [74]. (b) Long-term cycling capacity retention and corresponding coulombic efficiency of Zn//CuVO yarn battery at 5 A g<sup>-1</sup> at 60 °C. © Copyright 2022, American Chemical Society [76].

### 3.1.3. Hydrogel Electrolytes

For flexible energy storage systems, a gel electrolyte is particularly appealing compared to liquid electrolytes because of the following benefits [84]: (1) A gel electrolyte can stop liquid electrolytes from escaping (Ref. [90]); (2) A gel electrolyte may function as a separator by itself, making the construction of zinc-ion batteries simpler; (3) The sticky interface of the gel electrolyte may improve the electrodes' interfacial suitability and guarantee steady electrochemical performances; gel electrolytes with smart flexibility, self-healing properties, and stretchability might provide devices additional cutting-edge features (Ref. [91]); (4) A gel electrolyte might inhibit the creation of zinc dendrites (Ref. [92]); and (5) Gel electrolytes with smart responsiveness, a self-healing nature, and stretchability could give devices more innovative functions (Refs. [93–95]). To stabilize the H<sub>2</sub>O molecular network in the electrolyte, Liu et al. [76] developed a hydrogel electrolyte PNMT with a semi-interpenetrating cross-linked network structure based on polyacrylamide (PAM), cotton cellulose nanofibers (CNF), and carboxymethyl cellulose IV (CMC). This electrolyte displayed excellent mechanical properties, high sulfur conductivity, thermochemical cycling stability, and exceptional electrochemical performance. The battery utilizing this electrolyte demonstrated outstanding cycling stability at 25 °C, 40 °C, and 60 °C after 120 charge/discharge cycles, with capacity retention of 99%, 97%, and 96%, respectively. Moreover, the long-term cycling capacity retention of Zn//CuVO exceeded 200 mAh/g after 1200 cycles under high-temperature conditions (60 °C), and the corresponding coulombic efficiency of the Zn//CuVO-code cell remained close to 99% at 5A/g current (Figure 12b).

The aforementioned electrolyte strategies can enhance the electrochemical performance of AZIBs under specific temperature conditions (high or low temperature). However, to meet practical requirements, it is crucial to develop a wide-temperature-range electrolyte that can accommodate both high and low temperatures.

#### 4. Wide Temperature Condition

AZIBs encounter significant Zn cathode and electrolyte challenges at wide temperature operating conditions, leading to poor battery operability and suboptimal electrochemical performance. Consequently, understanding the failure mechanisms of AZIBs at various operating temperatures and developing AZIBs with stable operation under wide-temperature conditions are essential. In recent years, numerous studies have addressed wide-temperature AZIBs to advance both theoretical research and practical applications, where the major efforts have been devoted to regulating the hydrogen bonding network, simultaneously enabling the anti-freezing for low temperature and the inhibited H<sub>2</sub>O activity for high temperature. Table 3 shows the summary of electrochemical performance in AZIBs at wide temperature.

**Table 3.** The summary of electrochemical performance in AZIBs at wide temperature (anode: Zn).

Cathodes	Electrolytes	Temperature	Electrochemical Performance	Ref.
CuVO-300 <sup>a</sup>	ZnSO <sub>4</sub>	50 °C to 0 °C	410 mAh/g at 0.5 A/g at 50 °C 320 mAh/g at 0.5 A/g at 0 °C	[96]
δ-MgVO <sup>b</sup>	polyvinyl alcohol/glycerol gel-Zn(CF <sub>3</sub> SO <sub>3</sub> ) <sub>2</sub>	60 °C to −30 °C	308.7 mAh/g 153 mAh/g after 5000 cycles at 2A/g	[97]
Zn <sub>3</sub> V <sub>2</sub> O <sub>8</sub>	PAAm/DMSO/Zn(CF <sub>3</sub> SO <sub>3</sub> ) <sub>2</sub> <sup>c</sup>	60 °C to −40 °C	265.2 mAh/g after 3000 cycles at 0.2 A/g	[98]
Cu	Zn(BF <sub>4</sub> ) <sub>2</sub> /EG	40 °C to −30 °C	CE of 97.3%, 96.9% and 95.7% with good cycling stability (over 135, 100 and 100 cycles)	[99]
LiMn <sub>2</sub> O <sub>4</sub>	BM-gel <sup>d</sup>	80 °C to −20 °C	105 mAh/g after 150 cycles at 2.0 A/g at 80 °C 165 mAh/g at 0.2 A/g at −20 °C	[21]

(a) CuVO = CuxV<sub>2</sub>O<sub>5</sub>·nH<sub>2</sub>O; 300 = 300 °C; (b) δ-MgVO = Mg<sub>0.19</sub>V<sub>2</sub>O<sub>5</sub>·0.99H<sub>2</sub>O; (c) PAAm = polyacrylamide; DMSO = dimethyl sulfoxide; (d) BM-gel = biomimetic organohydrogel.

##### 4.1. Quasi-Solid-State Electrolytes

Zhou et al. [97] synthesized Mg<sub>0.19</sub>V<sub>2</sub>O<sub>5</sub>·0.99H<sub>2</sub>O (δ-MgVO) with large interlayer spacing using a pre-intercalation strategy and assembled a quasi-solid-state battery by pairing Zn/δ-MgVO as a cathode with a polyvinyl alcohol/glycerol gel electrolyte. This quasi-solid-state battery demonstrates satisfactory performance across a wide temperature range of −30 °C to 60 °C, making it suitable for environmentally adaptive aqueous energy storage devices. High capacities of 308.7, 269.7, 227, and 153 mAh/g are sustained at 60, 25, 0, and −30 °C, from high temperature to low temperature, respectively, after a cycle life test of 5000 cycles at 2 A/g (Figure 13a). The PVA/G battery can nevertheless offer high reversible capacities of 246.3, 226.4, 204.9, 176.1, and 136.7 mAh/g at current densities of 0.2, 0.5, 1, 2, and 5 A/g, respectively, even at a relatively low temperature of −30 °C (Figure 13b). Lu et al. [98] suggested that a multi-component cross-linked hydrogel electrolyte could suppress Zn dendrites and enable low-temperature environmental adaptation of ZIBs. Leveraging the inhibitory effect of polyacrylamide and dimethyl sulfoxide (DMSO) on Zn dendrites, the completed full-cell exhibits a large specific capacity of 265.2 mAh/g at current densities of 0.2 A/g and remarkable cyclic stability with a capacity retention of 95.27% after 3000 cycles. More importantly, the galvanostatic charge–discharge (GCD) curves measured at temperatures ranging from −40 °C to 60 °C indicate that the two-step charge storage mechanism of the charge/discharge process remains unchanged with temperature (Figure 13c,d).

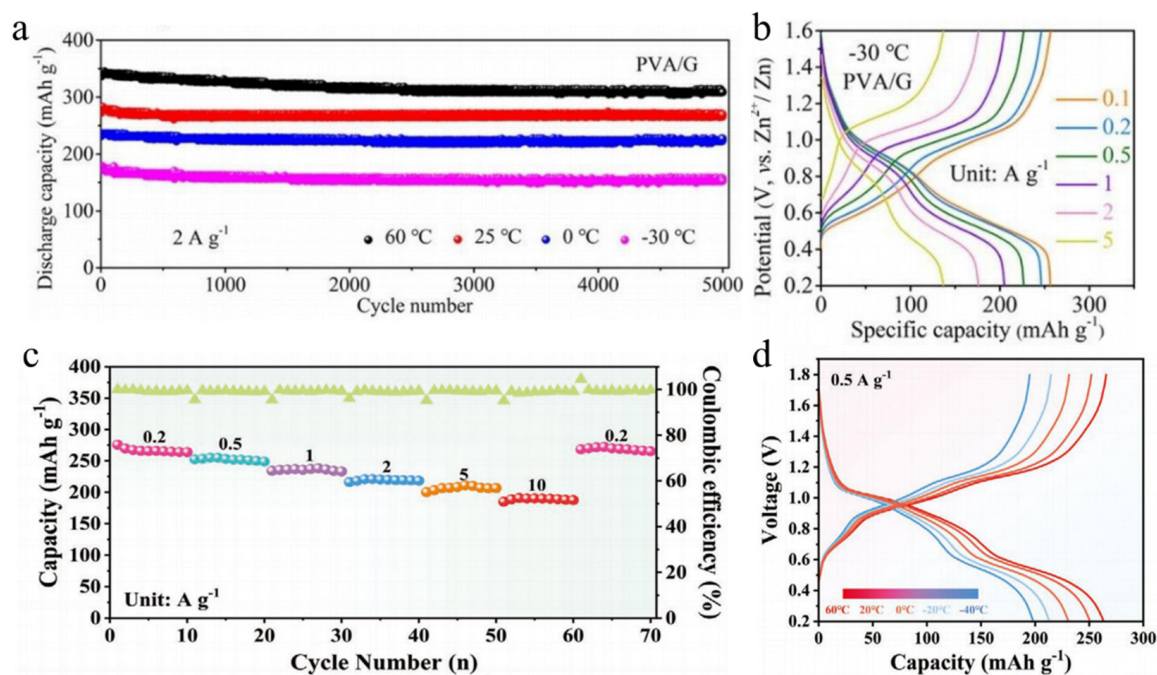


**Figure 13.** AZIBs performance at wide temperature condition. (a) The thin-film PVAG Zn $\delta$ -MgVO battery cycling performances at 2 A/g at different temperatures. (b) GCD curves at different current densities at  $-30\text{ }^{\circ}\text{C}$ . © Copyright 2020, Royal Society of Chemistry [97]. (c) Rate capability of Zn $_3$ V $_2$ O $_8$ Zn | PDZ-H full cell at different current densities. PAAm/DMSO/Zn(CF $_3$ SO $_3$ ) $_2$  multicomponent hydrogel electrolyte (defined as PDZ-H electrolyte). (d) GCD curves at different temperatures from  $60\text{ }^{\circ}\text{C}$  to  $-40\text{ }^{\circ}\text{C}$ . © Copyright 2022, Wiley-VCH GmbH [98].

#### 4.2. Organic Additives

By reducing the water content in the aqueous electrolyte and increasing the organic solvent, the hybrid aqueous–organic electrolyte is prepared with suppressed water activity, which also exhibits good performance over a wide temperature range. Han et al. [99] used EG as a solvent and added it into the water-containing organic electrolyte based on Zn(BF $_4$ ) $_2$ , which has accommodated flame retardancy. Due to the strong hydrogen bonding between various components, the electrolyte can not only effectively inhibit the dendrite reaction, corrosion, and hydrogen evolution reaction of the Zn anode in a wide operating temperature range, but it can also promote the formation of a favorable ZnF $_2$  passivation layer and form a certain protection mechanism. The electrochemical performance of Zn/Cu cells across a wide temperature range from  $40\text{ }^{\circ}\text{C}$  to  $-30\text{ }^{\circ}\text{C}$  was examined to determine the viability of the 4 M Zn(BF $_4$ ) $_2$ /EG electrolyte in challenging circumstances. The Zn||Cu battery using this electrolyte displayed a high CE of 97.3%, 96.9%, and 95.7% with good cycling stability (over 135, 100, and 100 cycles) at  $40\text{ }^{\circ}\text{C}$ ,  $-15\text{ }^{\circ}\text{C}$ , and  $-30\text{ }^{\circ}\text{C}$ , respectively (Figure 14a–c). In contrast, the electrochemical performance of the cell using the reference ZnSO $_4$  electrolyte exhibited poor CE properties for 95.8% and 47.1% along with a short term of sixty cycles, and only one cycle under the conditions of  $40\text{ }^{\circ}\text{C}$  and  $-15\text{ }^{\circ}\text{C}$ . In addition, the battery showed the worst performance, which was frozen, so that it could not work at  $-30\text{ }^{\circ}\text{C}$ . These results demonstrate the Zn(BF $_4$ ) $_2$ /EG electrolyte’s exceptional wide temperature performance. The interaction inside the electrolyte and the solvation structure of Zn $^{2+}$  were verified by DFT calculations and MD simulations. DFT calculations show that the relative binding energy between any two components obeys the order of magnitude of Zn $^{2+}$ -BF $_4^-$  > Zn $^{2+}$ -EG > Zn $^{2+}$ -H $_2$ O > BF $_4^-$ -EG > BF $_4^-$ -H $_2$ O > EG-H $_2$ O in 4 M Zn(BF $_4$ ) $_2$ /EG electrolyte (Figure 15a). MD simulations show that in 4 M Zn(BF $_4$ ) $_2$ /EG, three components (EG, H $_2$ O, and BF $_4^-$ ) are involved in the solvation sheath of Zn $^{2+}$  ions (Figure 15b,c).

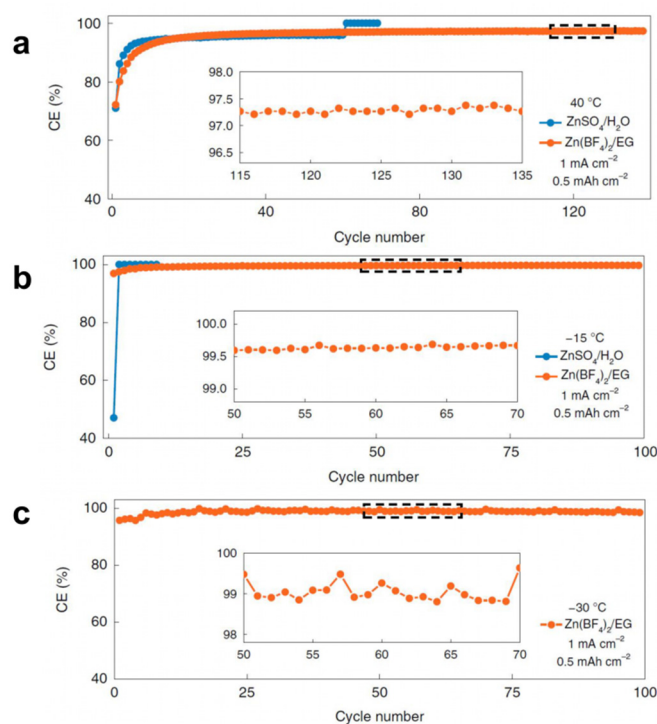


**Figure 14.** (a) Zn plating-stripping CE in the 4 m Zn(BF<sub>4</sub>)<sub>2</sub>/EG electrolyte at 40 °C. (b) Zn plating-stripping CE in the 4 m Zn(BF<sub>4</sub>)<sub>2</sub>/EG electrolyte at -15 °C. (c) Zn plating-stripping CE in the 4 M Zn(BF<sub>4</sub>)<sub>2</sub>/EG electrolyte at -30 °C. © Copyright 2021, The Author(s), Springer Nature Limited [99].

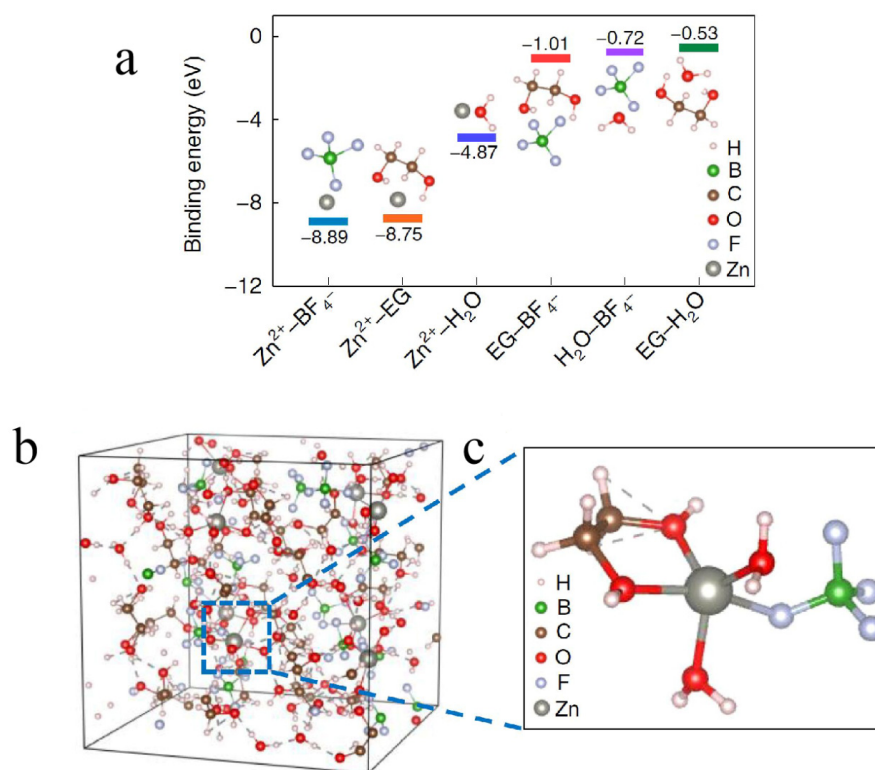


**Figure 15.** (a) Relative binding energies between any two ingredients in the Zn(BF<sub>4</sub>)<sub>2</sub>/EG electrolyte obtained from DFT calculations. (b) Snapshot of a typical MD-simulated cell for the 4 m Zn(BF<sub>4</sub>)<sub>2</sub>/EG electrolyte. (c) Representative Zn<sup>2+</sup> solvation structure in the 4 m Zn(BF<sub>4</sub>)<sub>2</sub>/EG electrolyte obtained from the MD simulation in (b). © Copyright 2021, The Author(s), Springer Nature Limited [99].

Mo et al. proposed a biomimetic organohydrogel (BM-gel) electrolyte, which can effectively and efficiently block water evaporation and seclude hydrogel from external surroundings. This BM-gel electrolyte kept up excellent electrochemical performance even at excessive temperatures (from 80 °C to −20 °C) in the Zn-MnO<sub>2</sub> battery, which exhibited a stable specific capacity of 105 mAh/g after 150 cycles at 2.0 A/g current density at 80 °C and a high specific capacity of 165 mAh/g at 0.2 A/g current density at subzero temperature -20 °C [21].

It can be seen that the electrolytes of AZIBs are modified by the above method, and quasi-solid electrolytes are the main means to achieve wide temperature range. The electrolytes need satisfy the characteristics of the high-temperature domain and the low-temperature domain, which greatly expands the application range of the AZIBs in various environments.

## 5. Summary and Outlook

The wide-temperature performance of AZIBs significantly impacts their practical applications. This review discussed the challenges and strategies associated with AZIBs under extreme conditions, such as low temperatures, high temperatures, and wide temperature ranges, where regulating the hydrogen bonding network and H<sub>2</sub>O activity is the effective strategy. Despite advancements in the field of wide-temperature AZIB electrolytes over the past three years, several obstacles remain. Based on the authors' knowledge and understanding, future research should focus on addressing the following challenges:

1. In addition to the development of wide-temperature electrolytes, self-protection represents another approach to enhance the wide-temperature performance of AZIBs [100,101]. Efficient thermal self-protection strategies for Zn-ion batteries using smart hygroscopic hydrogel electrolytes have been reported [97,102]. The reversible water evaporation and regeneration processes within the hydrogel are closely associated with temperature fluctuations, which can modulate ion migration in AZIB hydrogels. These findings present novel opportunities for creating environmentally adaptive aqueous energy storage devices with improved wide-temperature performance, driving future practical applications.
2. While AZIBs' operation at wide temperatures through intricate electrolyte design has been documented, the mechanisms underlying the entire battery system warrant a more comprehensive and systematic examination to better inform the practical application of AZIBs. Additionally, much of the current research on AZIBs remains confined to laboratory settings, with a considerable gap between these investigations and practical implementation. As such, achieving the real-world application of AZIBs necessitates the collective efforts of researchers worldwide.

**Author Contributions:** Conceptualization, G.L.; methodology, F.M. and H.H.; software, Z.S.; validation, L.S.; formal analysis, L.S.; investigation, L.S.; resources, C.D. and Q.W.; data curation, L.S.; writing—original draft preparation, L.S.; writing—review and editing, L.S. and Z.S.; visualization, Z.S.; supervision, G.L.; project administration, G.L.; funding acquisition, L.S., Z.S. and G.L. All authors have read and agreed to the published version of the manuscript.

**Funding:** This work was supported by the National Natural Science Foundation of China (No. 51972151 and 52171212). The authors gratefully acknowledge the financial support provided by the Shenzhen Municipality under the Stability Support Program of Shenzhen Colleges and Universities (GXWD20220817150352006) and the Project of Scientific Research Foundation for Returned Scholars (Grant No. DD11409018).

**Data Availability Statement:** There is no data support for this review.

**Conflicts of Interest:** The authors declare no conflict of interest.

## References

1. Armand, M.; Tarascon, J.M. Building better batteries. *Nature* **2008**, *451*, 652–657. [[CrossRef](#)] [[PubMed](#)]
2. Dunn, B.; Kamath, H.; Tarascon, J.M. Electrical energy storage for the grid: A battery of choices. *Science* **2011**, *334*, 928–935. [[CrossRef](#)] [[PubMed](#)]
3. Chen, M.; Zhang, Y.; Xing, G.; Chou, S.-L.; Tang, Y. Electrochemical energy storage devices working in extreme conditions. *Energy Environ. Sci.* **2021**, *14*, 3323–3351. [[CrossRef](#)]
4. Tang, Y.; Zhang, Y.; Li, W.; Ma, B.; Chen, X. Rational material design for ultrafast rechargeable lithium-ion batteries. *Chem. Soc. Rev.* **2015**, *44*, 5926–5940. [[CrossRef](#)] [[PubMed](#)]
5. Fu, Q.; Hao, S.; Meng, L.; Xu, F.; Yang, J. Engineering Self-Adhesive Polyzwitterionic Hydrogel Electrolytes for Flexible Zinc-Ion Hybrid Capacitors with Superior Low-Temperature Adaptability. *ACS Nano* **2021**, *15*, 18469–18482. [[CrossRef](#)] [[PubMed](#)]
6. Zhao, C.X.; Liu, J.N.; Yao, N.; Wang, J.; Ren, D.; Chen, X.; Li, B.Q.; Zhang, Q. Can Aqueous Zinc-Air Batteries Work at Sub-Zero Temperatures? *Angew. Chem.-Int. Ed.* **2021**, *60*, 15281–15285. [[CrossRef](#)]
7. Wang, M.; Emre, A.; Tung, S.; Gerber, A.; Wang, D.; Huang, Y.; Cecen, V.; Kotov, N.A. Biomimetic Solid-State Zn<sup>2+</sup> Electrolyte for Corrugated Structural Batteries. *ACS Nano* **2019**, *13*, 1107–1115. [[CrossRef](#)]
8. Yang, Z.; Zhang, J.; Kintner-Meyer, M.C.; Lu, X.; Choi, D.; Lemmon, J.P.; Liu, J. Electrochemical energy storage for green grid. *Chem. Rev.* **2011**, *111*, 3577–3613. [[CrossRef](#)]
9. Kundu, D.; Talaie, E.; Duffort, V.; Nazar, L.F. The emerging chemistry of sodium ion batteries for electrochemical energy storage. *Angew. Chem.-Int. Ed.* **2015**, *54*, 3431–3448. [[CrossRef](#)]
10. Goodenough, J.B. How we made the Li-ion rechargeable battery. *Nat. Electron.* **2018**, *1*, 204. [[CrossRef](#)]
11. Liu, J.; Zhang, J.-G.; Yang, Z.; Lemmon, J.P.; Imhoff, C.; Graff, G.L.; Li, L.; Hu, J.; Wang, C.; Xiao, J.; et al. Materials Science and Materials Chemistry for Large Scale Electrochemical Energy Storage: From Transportation to Electrical Grid. *Adv. Funct. Mater.* **2013**, *23*, 929–946. [[CrossRef](#)]
12. Yang, Q.; Qu, X.; Cui, H.; He, X.; Shao, Y.; Zhang, Y.; Guo, X.; Chen, A.; Chen, Z.; Zhang, R.; et al. Rechargeable Aqueous Mn-Metal Battery Enabled by Inorganic-Organic Interfaces. *Angew. Chem. Int. Ed. Engl.* **2022**, *61*, e202206471.
13. Liang, G.; Li, X.; Wang, Y.; Yang, S.; Huang, Z.; Yang, Q.; Wang, D.; Dong, B.; Zhu, M.; Zhi, C. Building durable aqueous K-ion capacitors based on MXene family. *Nano Res. Energy* **2022**, *1*, e9120002. [[CrossRef](#)]
14. Li, H.; Ma, L.; Han, C.; Wang, Z.; Liu, Z.; Tang, Z.; Zhi, C. Advanced rechargeable zinc-based batteries: Recent progress and future perspectives. *Nano Energy* **2019**, *62*, 550–587. [[CrossRef](#)]
15. Elia, G.A.; Marquardt, K.; Hoepfner, K.; Fantini, S.; Lin, R.; Knipping, E.; Peters, W.; Drillet, J.F.; Passerini, S.; Hahn, R. An Overview and Future Perspectives of Aluminum Batteries. *Adv. Mater.* **2016**, *28*, 7564–7579. [[CrossRef](#)]
16. Liu, X.; Fan, X.; Liu, B.; Ding, J.; Deng, Y.; Han, X.; Zhong, C.; Hu, W. Mapping the Design of Electrolyte Materials for Electrically Rechargeable Zinc-Air Batteries. *Adv. Mater.* **2021**, *33*, e2006461. [[CrossRef](#)]
17. Song, M.; Tan, H.; Chao, D.; Fan, H.J. Recent Advances in Zn-Ion Batteries. *Adv. Funct. Mater.* **2018**, *28*, 1802564. [[CrossRef](#)]
18. Marcus, Y. Ionic radii in aqueous solutions. *J. Solut. Chem.* **1983**, *12*, 271–275. [[CrossRef](#)]
19. Tansel, B. Significance of thermodynamic and physical characteristics on permeation of ions during membrane separation: Hydrated radius, hydration free energy and viscous effects. *Sep. Purif. Technol.* **2012**, *86*, 119–126. [[CrossRef](#)]
20. Kang, H.; Liu, Y.; Cao, K.; Zhao, Y.; Jiao, L.; Wang, Y.; Yuan, H. Update on anode materials for Na-ion batteries. *J. Mater. Chem. A* **2015**, *3*, 17899–17913. [[CrossRef](#)]
21. Mo, F.; Liang, G.; Wang, D.; Tang, Z.; Li, H.; Zhi, C. Biomimetic organohydrogel electrolytes for high-environmental adaptive energy storage devices. *EcoMat* **2019**, *1*, e12008. [[CrossRef](#)]
22. Yang, Q.; Liang, G.; Guo, Y.; Liu, Z.; Yan, B.; Wang, D.; Huang, Z.; Li, X.; Fan, J.; Zhi, C. Do Zinc Dendrites Exist in Neutral Zinc Batteries: A Developed Electrohealing Strategy to In Situ Rescue In-Service Batteries. *Adv. Mater.* **2019**, *31*, e1903778. [[CrossRef](#)] [[PubMed](#)]
23. Yang, Q.; Li, L.; Hussain, T.; Wang, D.; Hui, L.; Guo, Y.; Liang, G.; Li, X.; Chen, Z.; Huang, Z.; et al. Stabilizing Interface pH by N-Modified Graphdiyne for Dendrite-Free and High-Rate Aqueous Zn-Ion Batteries. *Angew. Chem. Int. Ed. Engl.* **2022**, *61*, e202112304. [[CrossRef](#)] [[PubMed](#)]
24. Ge, H.; Feng, X.; Liu, D.; Zhang, Y. Recent advances and perspectives for Zn-based batteries: Zn anode and electrolyte. *Nano Res. Energy* **2023**, *2*, e9120039. [[CrossRef](#)]
25. Liu, Z.; Luo, X.; Qin, L.; Fang, G.; Liang, S. Progress and prospect of low-temperature zinc metal batteries. *Adv. Powder Mater.* **2022**, *1*, 100011. [[CrossRef](#)]
26. Huang, J.; Dong, X.; Wang, N.; Wang, Y. Building low-temperature batteries: Non-aqueous or aqueous electrolyte? *Curr. Opin. Electrochem.* **2022**, *33*, 100949. [[CrossRef](#)]
27. Zhu, X.; Wang, L. Advances in materials for all-climate sodium-ion batteries. *EcoMat* **2020**, *2*, e12043. [[CrossRef](#)]
28. Holoubek, J.; Liu, H.; Wu, Z.; Yin, Y.; Xing, X.; Cai, G.; Yu, S.; Zhou, H.; Pascal, T.A.; Chen, Z.; et al. Tailoring Electrolyte Solvation for Li Metal Batteries Cycled at Ultra-Low Temperature. *Nat. Energy* **2021**, *2021*, 303–313. [[CrossRef](#)]
29. Peng, H.-J.; Huang, J.-Q.; Cheng, X.-B.; Zhang, Q. Review on High-Loading and High-Energy Lithium-Sulfur Batteries. *Adv. Energy Mater.* **2017**, *7*, 1700260. [[CrossRef](#)]
30. Li, H.; Chao, D.; Chen, B.; Chen, X.; Chuah, C.; Tang, Y.; Jiao, Y.; Jaroniec, M.; Qiao, S.Z. Revealing Principles for Design of Lean-Electrolyte Lithium Metal Anode via In Situ Spectroscopy. *J. Am. Chem. Soc.* **2020**, *142*, 2012–2022. [[CrossRef](#)]

31. Rodrigues, M.-T.F.; Babu, G.; Gullapalli, H.; Kalaga, K.; Sayed, F.N.; Kato, K.; Joyner, J.; Ajayan, P.M. A materials perspective on Li-ion batteries at extreme temperatures. *Nat. Energy* **2017**, *2*, 17108. [[CrossRef](#)]
32. Cho, Y.; Gabbar, H.A. Review of energy storage technologies in harsh environment. *Saf. Extrem. Environ.* **2019**, *1*, 11–25. [[CrossRef](#)]
33. Yang, X.G.; Zhang, G.; Ge, S.; Wang, C.Y. Fast charging of lithium-ion batteries at all temperatures. *Proc. Natl. Acad. Sci. USA* **2018**, *115*, 7266–7271. [[CrossRef](#)]
34. Abdellahi, A.; Urban, A.; Dacek, S.; Ceder, G. Understanding the Effect of Cation Disorder on the Voltage Profile of Lithium Transition-Metal Oxides. *Chem. Mater.* **2016**, *28*, 5373–5383. [[CrossRef](#)]
35. Lee, J.; Kitchaev, D.A.; Kwon, D.H.; Lee, C.W.; Papp, J.K.; Liu, Y.S.; Lun, Z.; Clement, R.J.; Shi, T.; McCloskey, B.D.; et al. Reversible Mn<sup>2+</sup>/Mn<sup>4+</sup> double redox in lithium-excess cathode materials. *Nature* **2018**, *556*, 185–190. [[CrossRef](#)]
36. Cui, H.; Ma, L.; Huang, Z.; Chen, Z.; Zhi, C. Organic materials-based cathode for zinc ion battery. *SmartMat* **2022**, *3*, 565–581. [[CrossRef](#)]
37. Liu, Y.; Liu, Y.; Yamauchi, Y.; Alothman, Z.A.; Kaneti, Y.V.; Wu, X. Enhanced Zinc Ion Storage Capability of V<sub>2</sub>O<sub>5</sub> Electrode Materials with Hollow Interior Cavities. *Batter. Supercaps* **2021**, *4*, 1867–1873. [[CrossRef](#)]
38. Kamenskii, M.A.; Eliseeva, S.N.; Kondratiev, V.V. The Electrochemical Performance of δ-MnO<sub>2</sub> Cathode Material for Aqueous Zinc-Ion Batteries: The Role of Current Collector. *ECS Trans.* **2021**, *105*, 135–142. [[CrossRef](#)]
39. Li, F.; Hu, X. Zinc Metal Energy Storage Devices under Extreme Conditions of Low Temperatures. *Batter. Supercaps* **2020**, *4*, 389–406. [[CrossRef](#)]
40. Sun, T.; Yuan, X.; Wang, K.; Zheng, S.; Shi, J.; Zhang, Q.; Cai, W.; Liang, J.; Tao, Z. An ultralow-temperature aqueous zinc-ion battery. *J. Mater. Chem. A* **2021**, *9*, 7042–7047. [[CrossRef](#)]
41. Shi, Y.; Chen, Y.; Shi, L.; Wang, K.; Wang, B.; Li, L.; Ma, Y.; Li, Y.; Sun, Z.; Ali, W.; et al. An Overview and Future Perspectives of Rechargeable Zinc Batteries. *Small* **2020**, *16*, e2000730. [[CrossRef](#)] [[PubMed](#)]
42. Gu, Y.; Liu, J.; Qu, S.; Deng, Y.; Han, X.; Hu, W.; Zhong, C. Electrodeposition of alloys and compounds from high-temperature molten salts. *J. Alloys Compd.* **2017**, *690*, 228–238. [[CrossRef](#)]
43. Wang, J.; Yang, Y.; Wang, Y.; Dong, S.; Cheng, L.; Li, Y.; Wang, Z.; Trabzon, L.; Wang, H. Working Aqueous Zn Metal Batteries at 100 °C. *ACS Nano* **2022**, *16*, 15770–15778. [[CrossRef](#)]
44. Zhang, S.S.; Xu, K.; Jow, T.R. The low temperature performance of Li-ion batteries. *J. Power Sources* **2003**, *115*, 137–140. [[CrossRef](#)]
45. Jaguemont, J.; Boulon, L.; Dubé, Y. A comprehensive review of lithium-ion batteries used in hybrid and electric vehicles at cold temperatures. *Appl. Energy* **2016**, *164*, 99–114. [[CrossRef](#)]
46. Goodenough, J.B. Rechargeable batteries: Challenges old and new. *J. Solid State Electrochem.* **2012**, *16*, 2019–2029. [[CrossRef](#)]
47. Zhu, G.; Wen, K.; Lv, W.; Zhou, X.; Liang, Y.; Yang, F.; Chen, Z.; Zou, M.; Li, J.; Zhang, Y.; et al. Materials insights into low-temperature performances of lithium-ion batteries. *J. Power Sources* **2015**, *300*, 29–40. [[CrossRef](#)]
48. Nian, Q.; Wang, J.; Liu, S.; Sun, T.; Zheng, S.; Zhang, Y.; Tao, Z.; Chen, J. Aqueous Batteries Operated at -50 °C. *Angew. Chem.-Int. Ed.* **2019**, *58*, 16994–16999. [[CrossRef](#)]
49. Matsumoto, M.; Saito, S.; Ohmine, I. Molecular dynamics simulation of the ice nucleation and growth process leading to water freezing. *Nature* **2002**, *416*, 409–413. [[CrossRef](#)]
50. Moore, E.B.; Molinero, V. Structural transformation in supercooled water controls the crystallization rate of ice. *Nature* **2011**, *479*, 506–508. [[CrossRef](#)]
51. Sosso, G.C.; Chen, J.; Cox, S.J.; Fitzner, M.; Pedevilla, P.; Zen, A.; Michaelides, A. Crystal Nucleation in Liquids: Open Questions and Future Challenges in Molecular Dynamics Simulations. *Chem. Rev.* **2016**, *116*, 7078–7116. [[CrossRef](#)] [[PubMed](#)]
52. Zhang, Q.; Ma, Y.; Lu, Y.; Li, L.; Wan, F.; Zhang, K.; Chen, J. Modulating electrolyte structure for ultralow temperature aqueous zinc batteries. *Nat. Commun.* **2020**, *11*, 4463. [[CrossRef](#)] [[PubMed](#)]
53. Huang, S.; Hou, L.; Li, T.; Jiao, Y.; Wu, P. Antifreezing Hydrogel Electrolyte with Ternary Hydrogen Bonding for High-Performance Zinc-Ion Batteries. *Adv. Mater.* **2022**, *34*, e2110140. [[CrossRef](#)]
54. Sun, T.; Zheng, S.; Du, H.; Tao, Z. Synergistic Effect of Cation and Anion for Low-Temperature Aqueous Zinc-Ion Battery. *Nano-Micro. Lett.* **2021**, *13*, 204. [[CrossRef](#)] [[PubMed](#)]
55. Du, H.; Wang, K.; Sun, T.; Shi, J.; Zhou, X.; Cai, W.; Tao, Z. Improving zinc anode reversibility by hydrogen bond in hybrid aqueous electrolyte. *Chem. Eng. J.* **2022**, *427*, 131705. [[CrossRef](#)]
56. Chang, N.; Li, T.; Li, R.; Wang, S.; Yin, Y.; Zhang, H.; Li, X. An aqueous hybrid electrolyte for low-temperature zinc-based energy storage devices. *Energy Environ. Sci.* **2020**, *13*, 3527–3535. [[CrossRef](#)]
57. Chen, M.; Zhou, W.; Wang, A.; Huang, A.; Chen, J.; Xu, J.; Wong, C.-P. Anti-freezing flexible aqueous Zn–MnO<sub>2</sub> batteries working at -35 °C enabled by a borax-crosslinked polyvinyl alcohol/glycerol gel electrolyte. *J. Mater. Chem. A* **2020**, *8*, 6828–6841. [[CrossRef](#)]
58. Wang, Y.; Chen, Y. A flexible zinc-ion battery based on the optimized concentrated hydrogel electrolyte for enhanced performance at subzero temperature. *Electrochim. Acta* **2021**, *395*, 139178. [[CrossRef](#)]
59. Mo, F.; Liang, G.; Meng, Q.; Liu, Z.; Li, H.; Fan, J.; Zhi, C. A flexible rechargeable aqueous zinc manganese-dioxide battery working at -20 °C. *Energy Environ. Sci.* **2019**, *12*, 706–715. [[CrossRef](#)]
60. Tamtogh, A.; Bahn, E.; Sacchi, M.; Zhu, J.; Ward, D.J.; Jardine, A.P.; Jenkins, S.J.; Fouquet, P.; Ellis, J.; Allison, W. Motion of water monomers reveals a kinetic barrier to ice nucleation on graphene. *Nat. Commun.* **2021**, *12*, 3120. [[CrossRef](#)]

61. Roberts, A.J.; Danil de Namor, A.F.; Slade, R.C. Low temperature water based electrolytes for MnO<sub>2</sub>/carbon supercapacitors. *Phys. Chem. Chem. Phys.* **2013**, *15*, 3518–3526. [[CrossRef](#)]
62. Tron, A.; Jeong, S.; Park, Y.D.; Mun, J. Aqueous Lithium-Ion Battery of Nano-LiFePO<sub>4</sub> with Antifreezing Agent of Ethyleneglycol for Low-Temperature Operation. *ACS Sustain. Chem. Eng.* **2019**, *7*, 14531–14538. [[CrossRef](#)]
63. Wu, Q.-L.; Zhao, S.-X.; Yu, L.; Zheng, X.-X.; Wang, Y.-F.; Yu, L.-Q.; Nan, C.-W.; Cao, G. Oxygen vacancy-enriched MoO<sub>3-x</sub> nanobelts for asymmetric supercapacitors with excellent room/low temperature performance. *J. Mater. Chem. A* **2019**, *7*, 13205–13214. [[CrossRef](#)]
64. Liu, Z.; Zhang, J.; Liu, J.; Long, Y.; Fang, L.; Wang, Q.; Liu, T. Highly compressible and superior low temperature tolerant supercapacitors based on dual chemically crosslinked PVA hydrogel electrolytes. *J. Mater. Chem. A* **2020**, *8*, 6219–6228. [[CrossRef](#)]
65. Yin, J.; Qi, L.; Wang, H. Anti-freezing aqueous electrolytes for electric double-layer capacitors. *Electrochim. Acta* **2013**, *88*, 208–216. [[CrossRef](#)]
66. Peng, S.; Jiang, X.; Xiang, X.; Chen, K.; Chen, G.; Jiang, X.; Hou, L. High-performance and flexible solid-state supercapacitors based on high toughness and thermoplastic poly(vinyl alcohol)/NaCl/glycerol supramolecular gel polymer electrolyte. *Electrochim. Acta* **2019**, *324*, 134874. [[CrossRef](#)]
67. Railanmaa, A.; Lehtimäki, S.; Keskinen, J.; Lupo, D. Non-toxic printed supercapacitors operating in sub-zero conditions. *Sci. Rep.* **2019**, *9*, 14059. [[CrossRef](#)]
68. Yue, F.; Tie, Z.; Deng, S.; Wang, S.; Yang, M.; Niu, Z. An Ultralow Temperature Aqueous Battery with Proton Chemistry. *Angew. Chem.-Int. Ed.* **2021**, *60*, 13882–13886. [[CrossRef](#)]
69. Jiang, H.; Shin, W.; Ma, L.; Hong, J.J.; Wei, Z.; Liu, Y.; Zhang, S.; Wu, X.; Xu, Y.; Guo, Q.; et al. A High-Rate Aqueous Proton Battery Delivering Power Below –78 °C via an Unfrozen Phosphoric Acid. *Adv. Energy Mater.* **2020**, *10*, 2000968. [[CrossRef](#)]
70. Li, C.; Li, P.; Yang, S.; Zhi, C. Recently advances in flexible zinc ion batteries. *J. Semicond.* **2021**, *42*, 101603. [[CrossRef](#)]
71. Liang, G.; Wang, Y.; Huang, Z.; Mo, F.; Li, X.; Yang, Q.; Wang, D.; Li, H.; Chen, S.; Zhi, C. Initiating Hexagonal MoO<sub>3</sub> for Superb-Stable and Fast NH<sub>4</sub><sup>+</sup> Storage Based on Hydrogen Bond Chemistry. *Adv. Mater.* **2020**, *32*, e1907802. [[CrossRef](#)]
72. Wang, H.; Chen, Z.; Ji, Z.; Wang, P.; Wang, J.; Ling, W.; Huang, Y. Temperature adaptability issue of aqueous rechargeable batteries. *Mater. Today Energy* **2021**, *19*, 100577. [[CrossRef](#)]
73. Hou, J.; Yang, M.; Wang, D.; Zhang, J. Fundamentals and Challenges of Lithium Ion Batteries at Temperatures between –40 and 60 °C. *Adv. Energy Mater.* **2020**, *10*, 1904152. [[CrossRef](#)]
74. Xie, X.; Fu, H.; Fang, Y.; Lu, B.; Zhou, J.; Liang, S. Manipulating Ion Concentration to Boost Two-Electron Mn<sup>4+</sup>/Mn<sup>2+</sup> Redox Kinetics through a Colloid Electrolyte for High-Capacity Zinc Batteries. *Adv. Energy Mater.* **2021**, *12*, 2102393. [[CrossRef](#)]
75. Yang, Y.; Tang, Y.; Fang, G.; Shan, L.; Guo, J.; Zhang, W.; Wang, C.; Wang, L.; Zhou, J.; Liang, S. Li<sup>+</sup> intercalated V<sub>2</sub>O<sub>5</sub>·nH<sub>2</sub>O with enlarged layer spacing and fast ion diffusion as an aqueous zinc-ion battery cathode. *Energy Environ. Sci.* **2018**, *11*, 3157–3162. [[CrossRef](#)]
76. Liu, Q.; Ji, Z.; Mo, F.; Ling, W.; Wang, J.; Lei, H.; Cui, M.; Zhang, Z.; Liu, Y.; Cheng, L.; et al. Stable Thermochromic Hydrogel for a Flexible and Wearable Zinc-Ion Yarn Battery with High-Temperature Warning Function. *ACS Appl. Energy Mater.* **2022**, *5*, 12448–12455. [[CrossRef](#)]
77. Wang, N.; Yang, Y.; Qiu, X.; Dong, X.; Wang, Y.; Xia, Y. Stabilized Rechargeable Aqueous Zinc Batteries Using Ethylene Glycol as Water Blocker. *ChemSusChem* **2020**, *13*, 5556–5564. [[CrossRef](#)]
78. Qiu, X.; Wang, N.; Dong, X.; Xu, J.; Zhou, K.; Li, W.; Wang, Y. A High-Voltage Zn-Organic Battery Using a Nonflammable Organic Electrolyte. *Angew. Chem. Int. Ed.* **2021**, *60*, 21025–21032. [[CrossRef](#)]
79. Du, W.; Ang, E.H.; Yang, Y.; Zhang, Y.; Ye, M.; Li, C.C. Challenges in the material and structural design of zinc anode towards high-performance aqueous zinc-ion batteries. *Energy Environ. Sci.* **2020**, *13*, 3330–3360. [[CrossRef](#)]
80. Wang, J.; Yang, Y.; Zhang, Y.; Li, Y.; Sun, R.; Wang, Z.; Wang, H. Strategies towards the challenges of zinc metal anode in rechargeable aqueous zinc ion batteries. *Energy Storage Mater.* **2021**, *35*, 19–46. [[CrossRef](#)]
81. Chao, D.; Zhou, W.; Xie, F.; Ye, C.; Li, H.; Jaroniec, M.; Qiao, S.Z. Roadmap for advanced aqueous batteries: From design of materials to applications. *Sci. Adv.* **2020**, *6*, eaba4098. [[CrossRef](#)] [[PubMed](#)]
82. Wang, X.; Zhang, Z.; Xi, B.; Chen, W.; Jia, Y.; Feng, J.; Xiong, S. Advances and Perspectives of Cathode Storage Chemistry in Aqueous Zinc-Ion Batteries. *ACS Nano* **2021**, *15*, 9244–9272. [[CrossRef](#)]
83. Verma, V.; Kumar, S.; Manalastas, W.; Srinivasan, M. Undesired Reactions in Aqueous Rechargeable Zinc Ion Batteries. *ACS Energy Lett.* **2021**, *6*, 1773–1785. [[CrossRef](#)]
84. Li, X.; Wang, H.; Sun, X.; Li, J.; Liu, Y.-N. Flexible Wide-Temperature Zinc-Ion Battery Enabled by an Ethylene Glycol-Based Organohydrogel Electrolyte. *ACS Appl. Energy Mater.* **2021**, *4*, 12718–12727. [[CrossRef](#)]
85. Deng, W.; Zhou, Z.; Li, Y.; Zhang, M.; Yuan, X.; Hu, J.; Li, Z.; Li, C.; Li, R. High-Capacity Layered Magnesium Vanadate with Concentrated Gel Electrolyte toward High-Performance and Wide-Temperature Zinc-Ion Battery. *ACS Nano* **2020**, *14*, 15776–15785. [[CrossRef](#)] [[PubMed](#)]
86. Chen, M.; Chen, J.; Zhou, W.; Han, X.; Yao, Y.; Wong, C.P. Realizing an All-Round Hydrogel Electrolyte toward Environmentally Adaptive Dendrite-Free Aqueous Zn-MnO<sub>2</sub> Batteries. *Adv. Mater.* **2021**, *33*, e2007559. [[CrossRef](#)]
87. Liu, C.; Xu, W.; Mei, C.; Li, M.-C.; Xu, X.; Wu, Q. Highly stable H<sub>2</sub>V<sub>3</sub>O<sub>8</sub>/Mxene cathode for Zn-ion batteries with superior rate performance and long lifespan. *Chem. Eng. J.* **2021**, *405*, 126737. [[CrossRef](#)]

88. Hou, Z.; Lu, Z.; Chen, Q.; Zhang, B. Realizing wide-temperature Zn metal anodes through concurrent interface stability regulation and solvation structure modulation. *Energy Storage Mater.* **2021**, *42*, 517–525. [[CrossRef](#)]
89. Zhou, J.; Yuan, H.; Li, J.; Wei, W.; Li, Y.; Wang, J.; Cheng, L.; Zhang, D.; Ding, Y.; Chen, D.; et al. Highly reversible and stable Zn metal anode under wide temperature conditions enabled by modulating electrolyte chemistry. *Chem. Eng. J.* **2022**, *442*, 136218. [[CrossRef](#)]
90. Chan, C.Y.; Wang, Z.; Jia, H.; Ng, P.F.; Chow, L.; Fei, B. Recent advances of hydrogel electrolytes in flexible energy storage devices. *J. Mater. Chem. A* **2021**, *9*, 2043–2069. [[CrossRef](#)]
91. Chen, F.; Xu, Z.; Wang, H.; Handschuh-Wang, S.; Wang, B.; Zhou, X. Bioinspired Tough Organohydrogel Dynamic Interfaces Enabled Subzero Temperature Antifrosting, Deicing, and Antiadhesion. *ACS Appl. Mater. Interfaces* **2020**, *12*, 55501–55509. [[CrossRef](#)]
92. Lu, W.; Xie, C.; Zhang, H.; Li, X. Inhibition of Zinc Dendrite Growth in Zinc-Based Batteries. *ChemSusChem* **2018**, *11*, 3996–4006. [[CrossRef](#)]
93. Li, Q.; Cui, X.; Pan, Q. Self-Healable Hydrogel Electrolyte toward High-Performance and Reliable Quasi-Solid-State Zn-MnO(2) Batteries. *ACS Appl. Mater. Interfaces* **2019**, *11*, 38762–38770. [[CrossRef](#)]
94. Huang, Y.; Liu, J.; Wang, J.; Hu, M.; Mo, F.; Liang, G.; Zhi, C. An Intrinsically Self-Healing NiCo | Zn Rechargeable Battery with a Self-Healable Ferric-Ion-Crosslinking Sodium Polyacrylate Hydrogel Electrolyte. *Angew. Chem. Int. Ed. Engl.* **2018**, *57*, 9810–9813. [[CrossRef](#)]
95. Huang, S.; Wan, F.; Bi, S.; Zhu, J.; Niu, Z.; Chen, J. A Self-Healing Integrated All-in-One Zinc-Ion Battery. *Angew. Chem. Int. Ed. Engl.* **2019**, *58*, 4313–4317. [[CrossRef](#)]
96. Yang, Y.; Tang, Y.; Liang, S.; Wu, Z.; Fang, G.; Cao, X.; Wang, C.; Lin, T.; Pan, A.; Zhou, J. Transition metal ion-preintercalated V<sub>2</sub>O<sub>5</sub> as high-performance aqueous zinc-ion battery cathode with broad temperature adaptability. *Nano Energy* **2019**, *61*, 617–625. [[CrossRef](#)]
97. Zhou, W.; Chen, J.; Chen, M.; Wang, A.; Huang, A.; Xu, X.; Xu, J.; Wong, C.-P. An environmentally adaptive quasi-solid-state zinc-ion battery based on magnesium vanadate hydrate with commercial-level mass loading and anti-freezing gel electrolyte. *J. Mater. Chem. A* **2020**, *8*, 8397–8409. [[CrossRef](#)]
98. Lu, H.; Hu, J.; Wang, L.; Li, J.; Ma, X.; Zhu, Z.; Li, H.; Zhao, Y.; Li, Y.; Zhao, J.; et al. Multi-Component Crosslinked Hydrogel Electrolyte toward Dendrite-Free Aqueous Zn Ion Batteries with High Temperature Adaptability. *Adv. Funct. Mater.* **2022**, *32*, 2112540. [[CrossRef](#)]
99. Han, D.; Cui, C.; Zhang, K.; Wang, Z.; Gao, J.; Guo, Y.; Zhang, Z.; Wu, S.; Yin, L.; Weng, Z.; et al. A non-flammable hydrous organic electrolyte for sustainable zinc batteries. *Nat. Sustain.* **2021**, *5*, 205–213. [[CrossRef](#)]
100. Li, H.; Wang, F.; Zhang, C.; Ji, W.; Qian, J.; Cao, Y.; Yang, H.; Ai, X. A temperature-sensitive poly(3-octylpyrrole)/carbon composite as a conductive matrix of cathodes for building safer Li-ion batteries. *Energy Storage Mater.* **2019**, *17*, 275–283. [[CrossRef](#)]
101. Chen, Z.; Hsu, P.-C.; Lopez, J.; Li, Y.; To, J.W.F.; Liu, N.; Wang, C.; Andrews, S.C.; Liu, J.; Cui, Y.; et al. Fast and reversible thermoresponsive polymer switching materials for safer batteries. *Nat. Energy* **2016**, *1*, 15009. [[CrossRef](#)]
102. Yang, P.; Feng, C.; Liu, Y.; Cheng, T.; Yang, X.; Liu, H.; Liu, K.; Fan, H.J. Thermal Self-Protection of Zinc-Ion Batteries Enabled by Smart Hygroscopic Hydrogel Electrolytes. *Adv. Energy Mater.* **2020**, *10*, 2002898. [[CrossRef](#)]

**Disclaimer/Publisher's Note:** The statements, opinions and data contained in all publications are solely those of the individual author(s) and contributor(s) and not of MDPI and/or the editor(s). MDPI and/or the editor(s) disclaim responsibility for any injury to people or property resulting from any ideas, methods, instructions or products referred to in the content.